

REVIEW

Open Access



Methane hydrate systems off South Makassar Basin, Indonesia

Feisal Dirgantara^{1*} , Susilohadi Susilohadi¹, Mohammad Andri Syahrir Iskandar^{2,3} and Yudha Arisandhy Sintuwardhana⁴

Abstract

Previous drilling and coring efforts have confirmed the presence of methane hydrates in the deepwater Makassar Strait of Indonesia. The strait, separated into the North Makassar Basin and South Makassar Basin, is situated on the thinned Eurasian continental crust that began to rift during the Middle Eocene. While past methane hydrates studies have focused on the northern basin, the southern region lacks equivalent investigation. This research employs legacy multi-channel seismic reflection and well logs data to decipher the methane hydrate systems and associated free methane in the South Makassar Basin. Identified through the interpretation of bottom simulating reflectors (BSRs), seafloor topography, and structural features on seismic reflection profiles are five primary play types: polygonal faults type, slope type, buried fold type, buried carbonate mound type, and sediment waves type. The distinctive characteristics of BSRs in this region can be summarized as follows: (1) predominantly located beneath topographic highs and basin depocenter, (2) typically displaying a series of high-amplitude dipping reflectors beneath BSRs, (3) the distribution of BSRs is not always continuous and is not always parallel to that of the seafloor, and (4) the presence of blanking reflection above BSRs is variable. These features suggest methane hydrate accumulation preferentially occurs beneath structural highs and in basin depocenters, likely due to the upward and lateral migration of buoyant, methane-rich fluids. Through the analysis of seismic amplitude distribution and reflection strength in relation to BSR depth, hydrocarbon distribution is categorized into methane-hydrate reservoirs above BSRs and free methane reservoirs below BSRs. A first-order estimation of methane resources via petrophysical approach and Monte Carlo simulation suggests approximately 105 trillion cubic feet (TCF) of methane resources.

Keywords Methane hydrates, Free methane, Bottom-simulating reflectors, Play types, Volumetric estimation, South Makassar Basin

Introduction

Substantial volumes of methane are naturally stored globally in submarine and permafrost environments, primarily in the form of solid, temperature-sensitive methane hydrates at relatively shallow depths. These deposits, subject to specific temperature and pressure conditions, extend from a few meters to hundreds of meters below the seafloor, rendering them highly susceptible to variations in ocean temperatures associated with climate change. Methane, a potent greenhouse gas, has been implicated in exacerbating global warming during previous hyperthermal periods (e.g., Dickens et al. (1995); Kvenvolden (1999); Schmidt and Shindell (2003)). Ruppel

*Correspondence:
Feisal Dirgantara
fdirgant@gmail.com

¹ Research Center for Geological Resources, National Research and Innovation Agency of Indonesia, Bandung, Indonesia

² Marine Geological Institute of Indonesia, Bandung, Indonesia

³ Earth Resources Engineering Department, Kyushu University, Fukuoka, Japan

⁴ Geophysics Program, Physics Department, Gadjah Mada University, Yogyakarta, Indonesia

and Kessler (2017) have posited that contemporary global warming is causing the destabilization of marine hydrates in the marine environments, although sediment and water column sinks mostly mitigate methane emissions to the atmosphere. Beyond its climatic implications, the extensive global accumulation of natural methane hydrates plays crucial roles in marine ecosystems. Methane dynamics within the subseafloor sustain intricate anaerobic microbial communities, while seafloor emissions from dissociating hydrates contribute to benthic chemosynthetic communities, drive the formation of authigenic carbonates (Prouty et al. 2016; McVeigh et al. 2018), and fuel water column aerobic oxidation processes (Garcia-Tigreros et al. 2021). Additionally, the correlation between fossil landslides and sediments containing methane hydrates suggests that both the formation and dissociation of these hydrates may impact seafloor stability, potentially leading to submarine landslides (Elger et al. 2018). The identification of areas with rich methane hydrates and mapping submarine landslide susceptibility can assist in pinpointing locations more susceptible to perturbation (Tan et al. 2023), particularly for offshore infrastructure development and risk assessment. Furthermore, ongoing research continues to explore methane hydrates as a potential transitional energy source towards a renewable energy future, especially in regions or nations lacking domestic fossil fuel reserves (e.g., Yamamoto 2022). This dual perspective, considering both environmental and energy-related aspects, underscores the significance of methane hydrates in current scientific discourse.

Contemporary exploration of methane hydrates originated with the identification of bottom-simulating reflectors (BSRs) in seismic reflection records (e.g., Markl et al. 1970). These reflections serve as thermodynamic boundaries between the free methane below and the stable of methane hydrates above. Despite Indonesia's extensive history of conventional petroleum exploration, the investigation of methane hydrates remains elusive. First attempt to investigate methane hydrate dates back to 1980 as part of the Deep Sea Drilling Project conducted in the Timor Trough, where the presence of dissociated biogenic methane hydrates was verified via isotope analysis (McKirdy and Cook 1980). In the western part of Indonesia, the existence of methane hydrates in the Sunda convergent margin has been suggested based on the widespread occurrence of BSRs (Kopp 2002; Bahar et al. 2006; Lutz et al. 2011; Mukti et al. 2012). Chopra (1985) identified methane hydrates in the Andaman Sea near Sumatra through seismic reflection analysis, a discovery later validated by the Indian National Gas Hydrate Program Expedition 01 drilling (Collett et al. 2008). Likewise, the presence of methane hydrates has been inferred

in eastern Indonesia, such as in the Celebes Sea (Delisle et al. 1998; Neben et al. 1998), the Kutai Basin (Zhang and Wright 2017), and the Aru region (Priyanto et al. 2015). Even though Indonesia has abundant water bodies that account for roughly 81% of its overall area, there is limited scientific interest in offshore methane hydrates, evident from only around 17 published references on this subject over the past 44 years (Fig. 1).

In 2021, the Ministry of Energy and Mineral Resources of Indonesia asserted the potential reserves of methane hydrate, estimating a volume exceeding 850 trillion cubic feet (TCF), with the Makassar Strait being one of potential areas. The region has been a focal point for hydrocarbon exploration and production initiatives since the identification of oil in the Kutai Basin in 1897 (Yergin 1991). Jackson (2004) conducted the initial assessments of methane hydrates and free methane volumes in the North Makassar Basin (NMB), determining an estimated volume of 80 TCF. The validation was subsequently confirmed through deepwater drilling activities targeting conventional petroleum exploration, which penetrated methane hydrate layers in both the NMB and South Makassar Basin (SMB) in later years (Bacheller III et al. 2011; de Man et al. 2011, Courel et al. 2011). Tharimela and Filipov (2018) used a combination of seismic reflection and controlled-source electromagnetics data to identify high-resistivity methane hydrate zones above BSRs in the western NMB. Indications of active petroleum systems in the Makassar Strait are evidenced by hydrocarbon seepages identified through an airborne laser fluorescence survey (Thompson et al. 1991) and the discovery of adjacent gas fields (Courel et al. 2011). However, unlike its northern counterpart, the SMB lacks a comprehensive understanding of its methane hydrates development. This study aims to elucidate the methane hydrate systems in the SMB, including the first-order volumetric estimations using seismic reflection and well log data. Understanding the spatial distribution of methane hydrates is crucial for energy security and sustainability, aligning with the Indonesian government's objectives of reducing greenhouse gas emissions by 29% by 2030 through the use of natural gas as a cleaner energy source and eventually achieving net-zero emissions by 2060 (United Nation, 2022).

Regional geology

The Makassar Strait, opened since the Middle Eocene, lies to the southeast of the Eurasian lithosphere, between Kalimantan and Sulawesi islands. It acts as a distinct geographical divider, distinguishing the stable cratonic landmass of western Indonesia from the intricate archipelago of eastern Indonesia (Fig. 2). To the north, the strait is demarcated by the Palu-Koro fault, which separates it

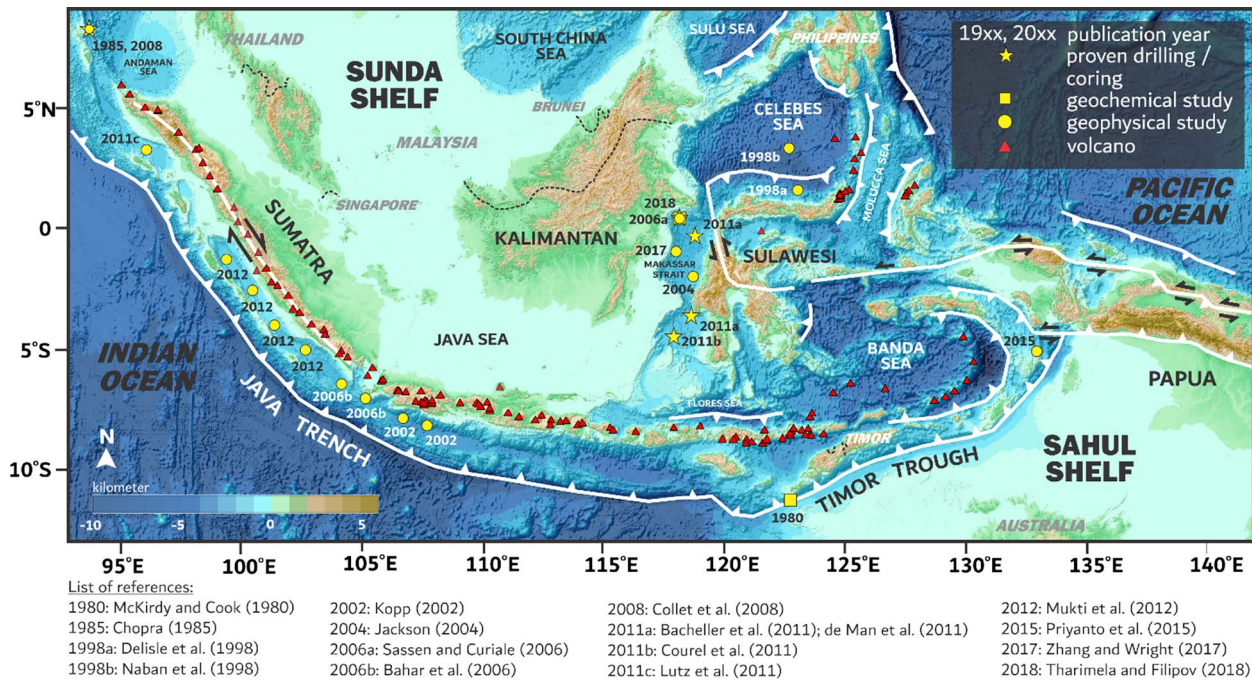


Fig. 1 Regional tectonic framework of Indonesia and adjacent countries overlain by location of methane hydrate studies between 1980 and 2024. Yellow-colored symbols represent references related to methane hydrates observation based on geochemical studies (square, e.g., McKirdy and Cook 1980); geophysical studies (circle, e.g., Chopra 1985), and drilling/coring report (star, e.g., Bacheller et al. 2011.). Red triangle infers the distribution of volcanoes. Dashed black lines are land political country borders

from the Sulawesi Sea. To the south, Spermonde islands and Masalima High bounds the strait (Hidayat et al. 2012). It is further divided into the NMB and the SMB by Paternoster Platform. Within both basins, a thick and relatively undisturbed sequence of Neogene and Paleogene sediments with excellent lateral continuity is present (Guntoro 1999).

The regional stratigraphy comprises three interconnected tectonic phases: syn-rift, post-rift, and compressional events (Longley 1997; Doust and Noble 2008; Kupecz et al. 2013) (Fig. 3). During the Middle Eocene rifting phase, significant tectonic activity resulted in a tilted basement block landscape filled with syn-rift clastic deposits consisting of volcanics, sands, coals, and shales, which contributed to the deposition of major Tertiary sediments. By the Late Eocene period, rising sea levels led to the formation of carbonate deposits. Subsequently, rapid development of ultra-deepwater conditions at the basin's center occurred due to extensive subsidence, causing sedimentation rates to lag and resulting in the accumulation of a thick, shaly Neogene overburden layer (Courel et al. 2011). In the Oligocene, the rifting activity ceased thereafter, leaving the thinned continental lithosphere existing without the development of a new oceanic crust (Hall et al. 2009).

The entire SMB had a significant deepening during the Oligocene when the depositional environment transformed into a basinal plain (Hidayat et al. 2012). Banggai Plate's westward movement into its current position and the subsequent compressional movement resulting from the collision with the East Sulawesi Ophiolite Belt in the Late Miocene (Davies 1990). Additionally, the convergence introduced Australian microcontinents that drifted against the eastern margin of the Makassar Strait, leading to the uplift of the West Sulawesi Fold Belt (WSFB) since the Early Pliocene and the subsequent formation of a series of foreland basin (Fraser et al. 2003; Bailie et al. 2004; Nur A'ini et al. 2005). In the southwestern part of strait, Armandita et al. (2015) reported the development of Late Miocene–Early Pliocene mass transport complex, covering an area of at least 9,000 km².

Historically, the Makassar Strait has been long considered an important hydrocarbon province in Indonesia, including the latest giant gas reservoir discovery of the Geng North field (S&P Global Commodity Insights, 2023) in the NMB. On the other hand, the SMB is an underdeveloped frontier basin with hydrocarbon potential (Courel et al. 2011). Despite the unsuccessful deep-water conventional petroleum drillings (e.g., Bacheller III et al. 2011; de Man et al. 2011), pervasive distribution of offshore hydrocarbon leakages has been suggested

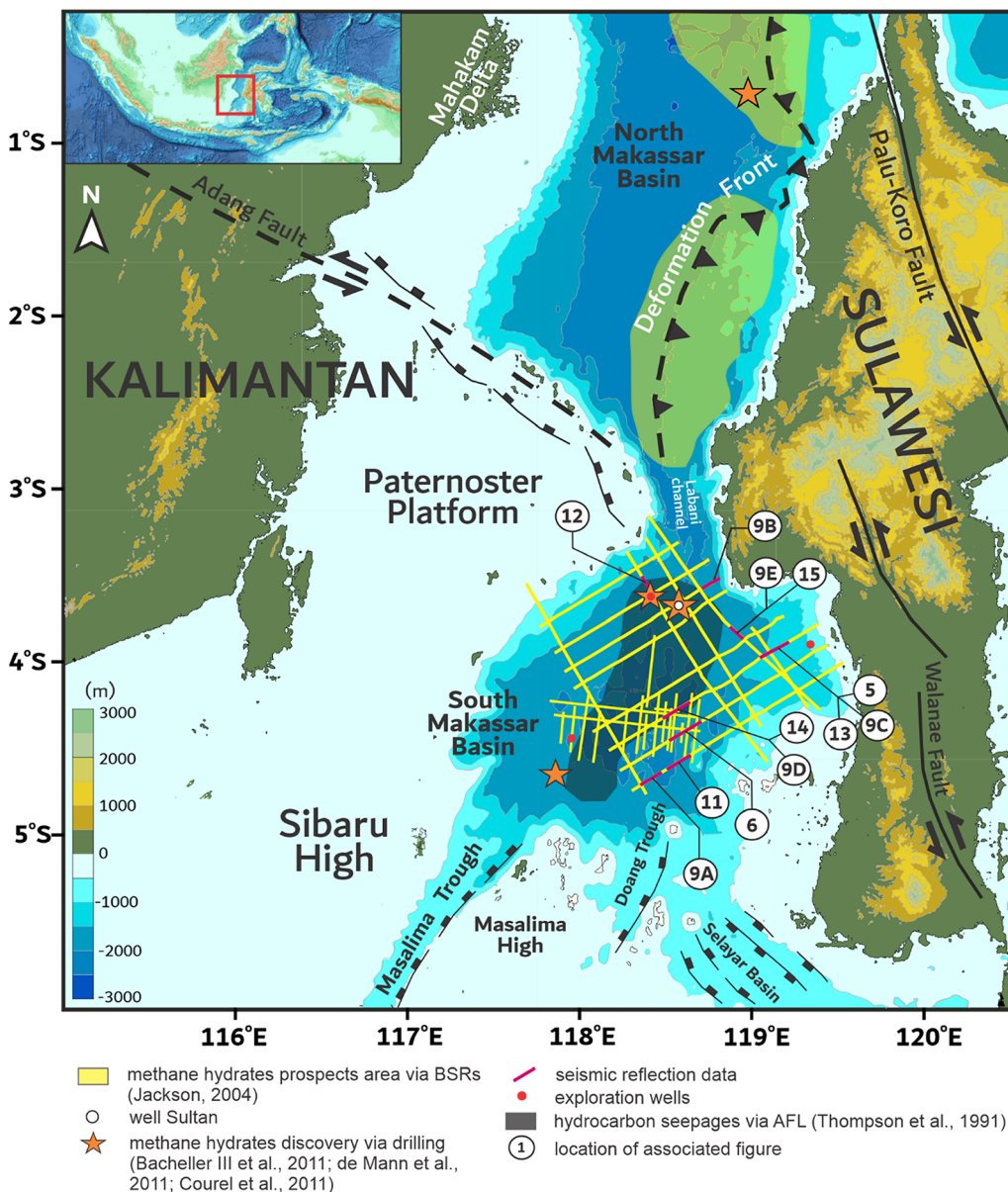


Fig. 2 The regional geology and tectonic framework of the Makassar Strait. The study area is situated in the South Makassar Basin (SMB). Numerous methane hydrate discoveries were found during deepwater drilling campaigns in 2011, as shown in orange star symbol. Dark lines with circled numbers show the locations of respective seismic sections appear in the corresponding figures in this paper. The red square in the inset map shows the location of the main map of the SMB

(Thompson et al. 1991; Courel et al. 2011). The study area is also characterized by geothermal gradients between 73 °C/km—84 °C/km (Nurusman and Subono 1995; Dirgantara et al. 2025, *in press*). The elevated geothermal gradients are likely linked to the thermal uplift from the deep mantle beneath the thinned Eurasian lithosphere (Zhang et al. 2021).

Methodology

Seismic reflection data

This research made use of 32 existing sets of two-dimensional (2D) multi-channel seismic data. These datasets, sourced from the Marine Geological Institute of Indonesia, cover an expanse of 14,670 km² and extend along a total line length of 2,400 km (Fig. 2). Primarily collected between 1969 and 2002, during the preliminary seismic survey in the Makassar Strait for

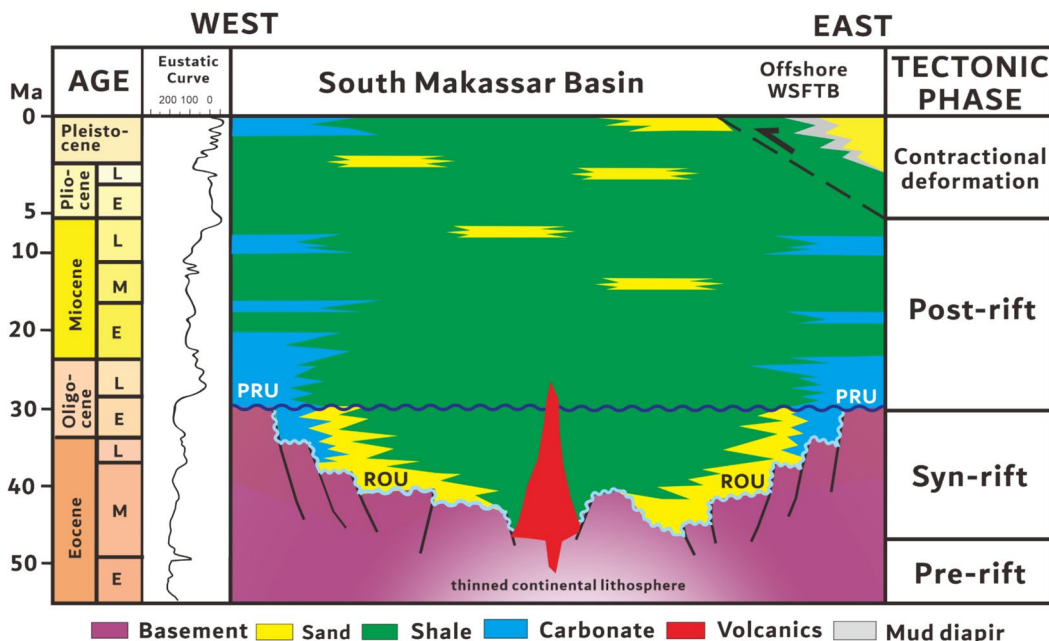


Fig. 3 Simplified stratigraphy of South Makassar Basin. ROU=rift onset unconformity. PRU=post-rift unconformity

identifying deepwater conventional petroleum targets, the seismic data underwent various standard processing procedures typical in the petroleum industry. These procedures included trace reformatting and editing, geometry configuration, spherical divergence, high-pass filtering, frequency–wave number (F-K) domain filtering, deconvolution, velocity analysis, correction for normal moveout (NMO) and dip moveout (DMO), residual velocity analysis, offset weighting, stacking, application of time and space variant filters, trace equalization, finite difference migration, and water column muting. With seismic records lasting a maximum of 10 s, these data encompass the continental slope, continental rise, and abyssal plain of the SMB. Additionally, this study utilized bathymetric data with a resolution of 15-arc seconds from the General Bathymetric Chart of the Oceans (GEBCO 2023).

Three types of seismic attributes were utilized to reveal the distribution of methane hydrates and free methane compartments: envelope, root mean square (RMS) amplitude, and sweetness. Historically, these attributes have been used in methane hydrate studies (e.g., Clairmont et al. 2021; Monteleone et al. 2022; Dirgantara et al. 2020a). Envelope attribute, also known as instantaneous amplitude, was utilized to measure the reflectivity strength as it displayed a direct proportional to the square root of the total energy of seismic signal at a particular moment in time (Holdaway 2014). RMS amplitude was utilized to showcase reflectivity zones in the area of

interest by measuring the magnitude of variation over a dataset (Holdaway 2014) by emphasizing the variations in acoustic impedance over a selected sample interval. Trace envelopes were often used to detect gas accumulation, and bright/dim/flat spots (Chen and Sidney 1997). By dividing instantaneous amplitude with square root of the instantaneous frequency, the sweetness attribute aimed to highlight anomalies by dimming out the high frequencies effects within the data (Kumar et al. 2018).

Well log data

Despite the presence of numerous exploration wells in the SMB (Fig. 2), only well Sultan was utilized due to its available log recordings extending to the depth of methane hydrate formation. The well was drilled as part of the conventional petroleum exploration campaign in the deepwater off SMB in 2009 and penetrated the abyssal plain of the basin at a water depth of 1,978 m. The well records gamma-ray, resistivity, and sonic logs with maximum penetration records down to 3,559 m. Based on the drilling report, seafloor temperature was recorded at 3.65 °C with base depth of theoretical methane hydrate formation reaching 2,176 m below sea surface. Dirgantara et al. (2025, *in press*) calculated a geothermal gradient of 71 °C/km for the well, noting a 19-m discrepancy in the depth of the methane hydrate stability zone (MHSZ) at 2,195 m compared to the depth reported in the drilling data.

The Wyllie time-average relationship (Wyllie et al. 1956) is used to calculate total porosity (ϕ_t) and effective porosity (ϕ_E) from transit times, based on the estimation of porosity derived from the calculation of the time-averaged velocity of wave propagation through porous media. The equations utilized for total porosity and effective porosity estimation are applied to both the MHSZ and free methane zone (FMZ) as follows:

$$\phi_t = \frac{\Delta t - \Delta t_{ma}}{\Delta t_f - \Delta t_{ma}} \quad (1)$$

$$\phi_{tsh} = \frac{\Delta t_{sh} - \Delta t_{ma}}{\Delta t_f - \Delta t_{ma}} \quad (2)$$

$$\phi_E = \phi_t - V_{sh} \cdot \phi_{tsh} \quad (3)$$

where Δt is compressional slowness ($\mu\text{s}/\text{ft}$) from sonic log, Δt_{ma} represents the transit time through the rock matrix, where acoustic waves travel through the solid framework of the rock, characterized by a compressional matrix slowness of 58 $\mu\text{s}/\text{ft}$, and Δt_f represents the transit time through fluid-filled pores, with a compressional slowness for the fluid of 189 $\mu\text{s}/\text{ft}$. Equation 2 estimates

the porosity of shale (ϕ_{tsh}), where Δt_{sh} is compressional slowness of shale. ϕ_E is estimated by subtracting the volume of clay-bound water from the total porosity, where V_{sh} is shale volume. Water resistivity (R_w) can be calculated following Dewan (1983):

$$R_w = \phi_E^2 R_t \quad (4)$$

Given that the drilling report identified Pleistocene shale formation as the main reservoir at the MHSZ depth, this study assumes shale to be the primary lithology in both MHSZ and FMZ. The true formation resistivity (R_t) is determined from the deep resistivity logs by defining ϕ_E greater than 10% and V_{sh} less than 35%, in order to exclude tight zones that could produce false hydrocarbon-like responses. The modified Simandoux relationship is used to estimate water saturation (S_w) in shale formation within both the MHSZ and FMZ:

$$\frac{\phi_E^m}{a \cdot R_w} S_w^n + \frac{V_{sh}}{R_{sh}} \cdot S_w - \frac{1}{R_t} = 0 \quad (5)$$

where tortuosity factor (a) accounts for influence of clay content, cementation exponent (m) reflects the relationship between resistivity and fluid saturation, and

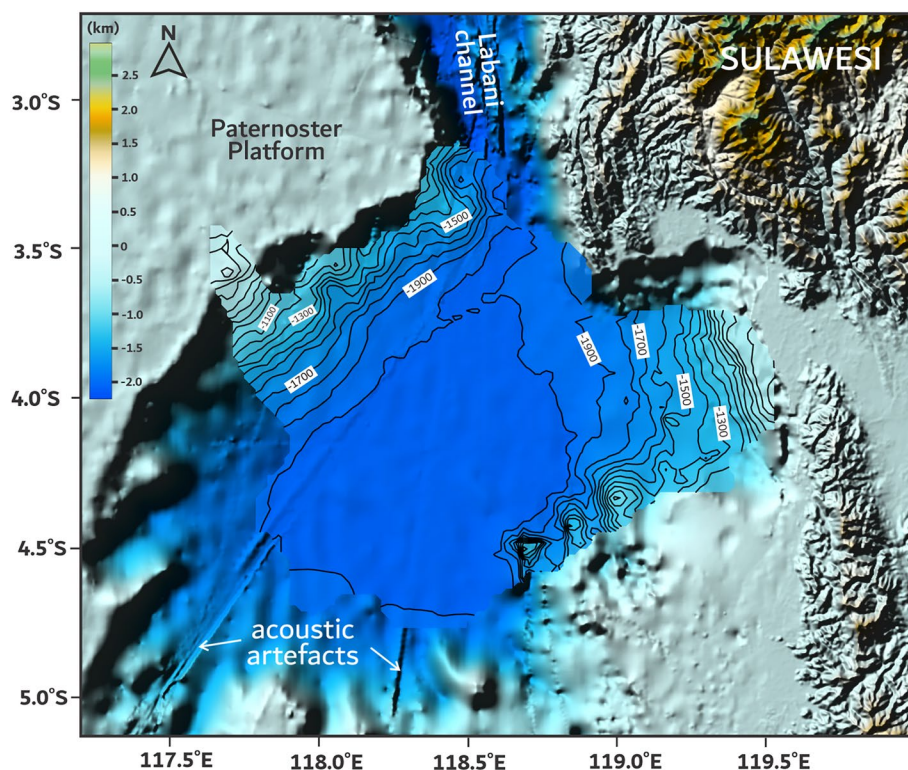


Fig. 4 The bathymetric features of the study area, as determined through seismic interpretation (contoured polygon), align closely with data from the General Bathymetric Chart of the Oceans (GEBCO 2023). The study area primarily encompasses the abyssal plain, with its lowest point reaching a depth of 2050 m. Acoustic artefacts are artificial seafloor topography from GEBCO data

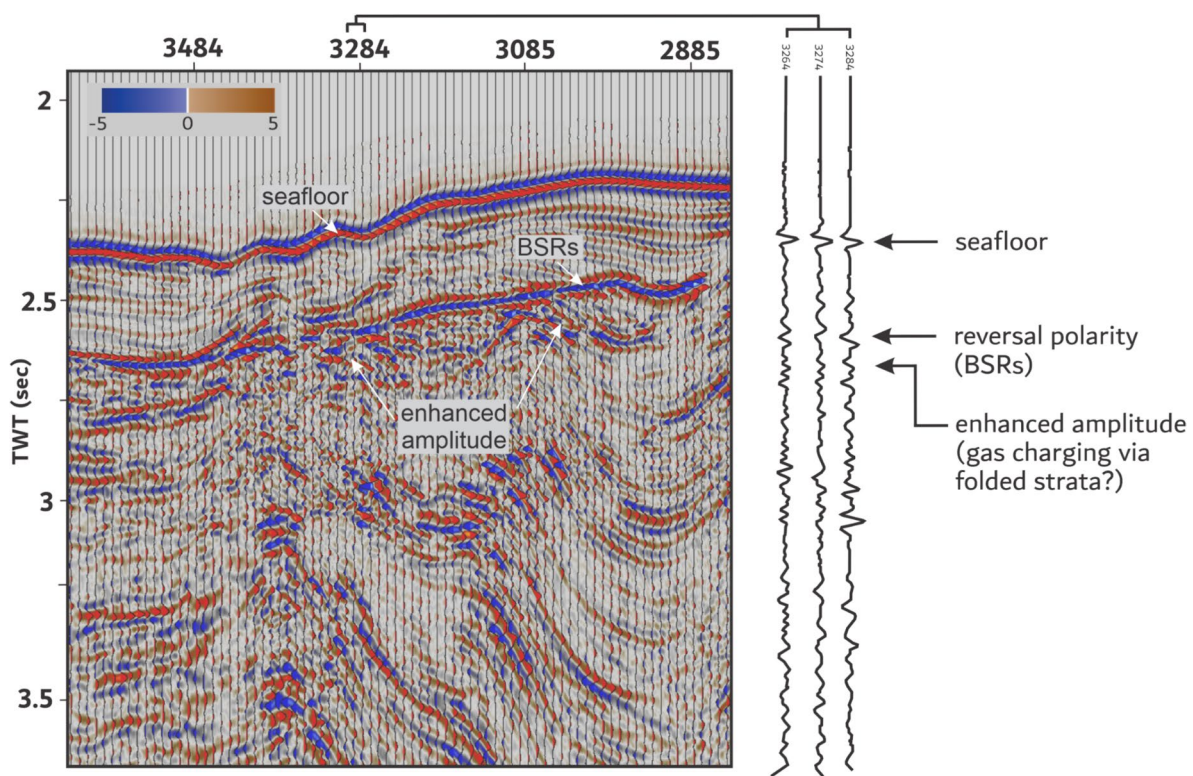


Fig. 5 A portion of the seismic profile in the research area displays the characteristics of BSRs, which exhibit polarity opposite to that of the seafloor and intersect with tilted reflections. Red-colored amplitudes represent positive reflection coefficients, while blue-colored ones indicate negative reflection coefficients. The extracted wavelets on the right exhibit seismic amplitudes alongside their respective interpretations. Refer to Fig. 2 for the location reference

saturation exponent (n) characterizes the relationship between fluid saturation and electrical resistivity or conductivity in the porous media, are assumed to be 1, 2, and 2, respectively. The resistivity of shale (R_{sh}) refers to the resistance of shale to electrical flow, with a value range of 40–60 $\Omega \cdot m$.

Volumetric estimation

Volumetric estimation provides a static measurement of in-place methane that is trapped within the hydrates and free methane below the hydrates. Analogous to that of conventional petroleum industry, original methane hydrate in place (OMHIP) and original free methane in place (OFMIP) are introduced to evaluate in-place hydrocarbons in the study area adopting the volumetric estimation in Dirgantara et al. (2020a), as follows:

$$H \cdot A \cdot \phi_E \cdot S_{mh} \cdot N/G \cdot VR \cdot CO \cdot (1/28,300) \text{ (OMHIP)} \quad (6)$$

$$H \cdot A \cdot \phi_E \cdot S_{fm} \cdot N/G \cdot (1/B_g) \cdot (1/28,300) \text{ (OFMIP)} \quad (7)$$

where H is gross thickness of possible methane hydrate or free methane occurrence; A is area coverage of potential

methane hydrate or free methane (km^2); S_{mh} is saturation of methane hydrate; S_{fm} is saturation of free methane; N/G is ratio between thickness of methane hydrate or free methane layer over gross thickness; VR is volume ratio of methane hydrate and natural methane converted from hydrate (164 at $0^\circ C$ and 1 atm); CO is cage occupancy of methane occupied in hydrate; B_g is gas formation volume factor; and $1/28,300$ is conversion unit to TCF (1 TCF = 28,300 Mm^3).

This study assumes that both OMHIP and OFMIP assume S_w is the only alternative fluid besides S_{mh} and S_{fm} that constitutes each reservoir. This leads to the relationship of

$$S_w + S_{mh} = 1 \text{ (for methane hydrate reservoir)} \quad (8)$$

$$S_w + S_{fm} = 1 \text{ (for free methane reservoir)} \quad (9)$$

The study area boundaries are established by extrapolating the interpreted BSRs across the entire area, while the thickness is assumed to remain constant based on the methane hydrate thickness recorded in the drilling report of well Sultan, which is reported as 198 m. As OFMIP

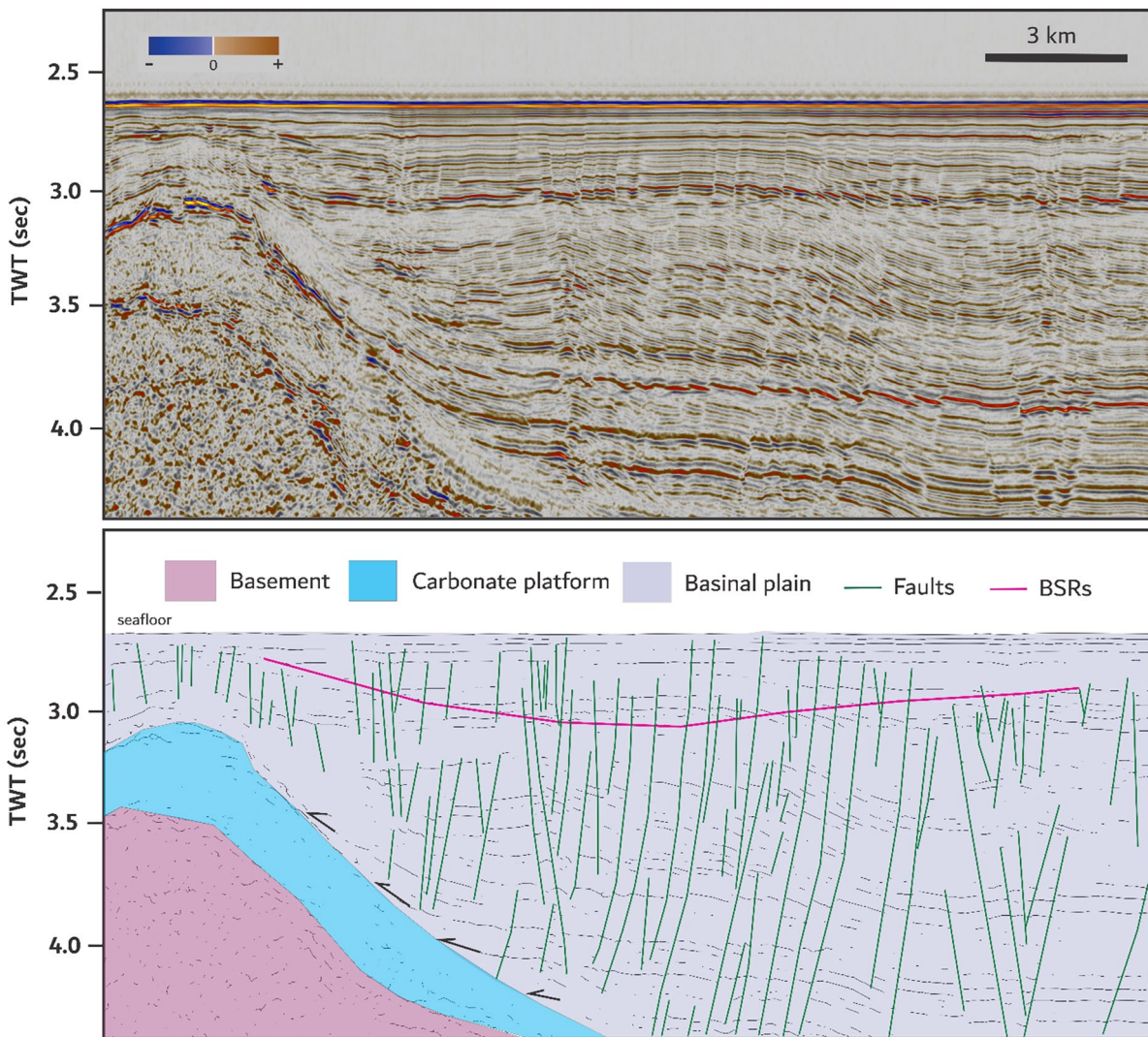


Fig. 6 The seismic sections, both uninterpreted (above) and interpreted (below), illustrate that BSRs do not always consistently align parallel to the bedding of the seafloor. Refer to Fig. 2 for location

estimation follows the conventional original methane in place approach, one of key parameters in Eq. 7 is B_g , which is dependent on temperature (in Rankine scale, °R), pressure, and gas composition of the reservoir. B_g relates gas volume at reservoir conditions to volume at standard conditions and is described as follows:

$$B_g = \frac{V_r}{V_s} = \frac{P_s n Z R T_r}{P_r n Z_s R T_s} = \frac{Z T_r P_s}{P_r T_s} \quad (10)$$

where V_r is gas volume under reservoir condition, V_s is gas volume in surface condition, P_s is standard atmospheric pressure (14.7 psi), P_r is reservoir pressure (psi), n is amount of gas substance (moles), Z is gas compressibility factor, Z_s is standard gas compressibility factor (=1), R is gas constant (8.31441 J/K.mol), T_r is temperature at

reservoir condition (°R), and T_s is temperature at standard condition (=520 °R).

Equation 10 suggests three non-constant parameters (Z , P_r , and T_r). For non-ideal gas, Z can be calculated under gas critical point based on thermodynamics equation of state from Peng and Robinson (1976), known as Peng–Robinson equation, as follows:

$$P = \frac{RT}{v - b} - \frac{\alpha(T)}{v(v + b) + b(v - b)} \quad (11)$$

where P is pressure (psi), T is absolute temperature (°K), α is attraction parameter, v is molar volume (m^3/mol), and b is van der Waals volume (m^3/mol). Elliott and Lira (2012) solves the Peng–Robinson equation for Z under given gas critical constants, acentric factor, pressure,

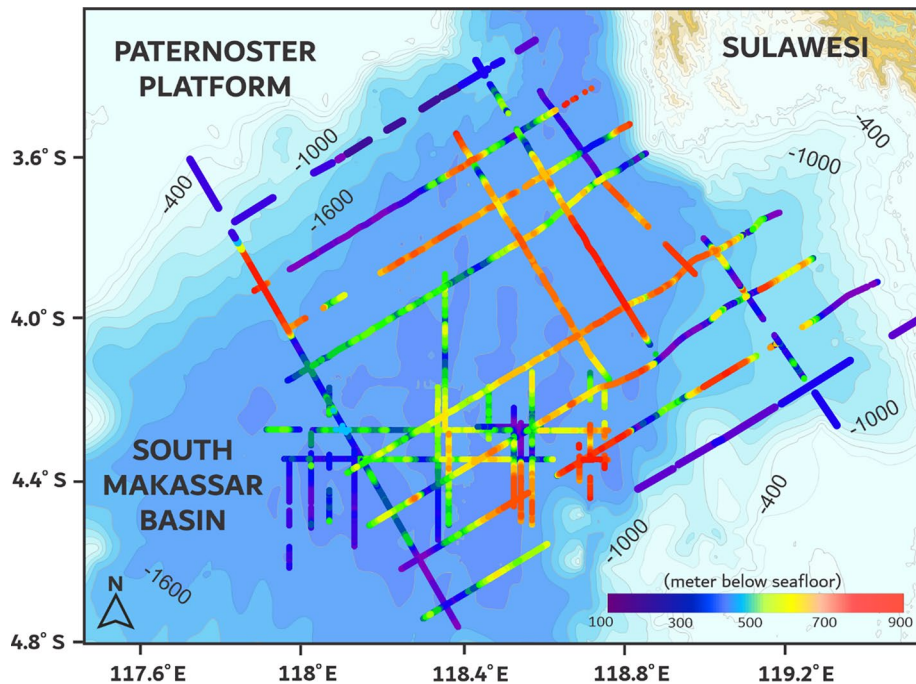


Fig. 7 The distribution of BSRs is superimposed on bathymetry data, revealing that BSRs are primarily concentrated in three main areas: the topographic highs, the basin depocenter, and along the basin margin. These BSRs are situated at depths ranging between 100 to 900 m below the seafloor

and temperature constraints. In order to derive reservoir pressure, Hamilton (1980) estimation of sub-bottom depth based on seismic travel time is implemented and is described as follows:

$$Z = 1511t + 1041t^2 - 372t^3 \quad (12)$$

where Z is depth of interest (m), t is one-way travel time below sea floor (s). This relationship has been utilized by previous studies in the western marginal basin off the Pacific Ocean (e.g., Schnurle et al. 1999). Since methane hydrate and associated free methane reservoirs are situated at relatively shallow depth, the reservoirs pressure is assumed to be constrained mainly by hydrostatic pressure, P_r , with minimal influence of pore pressure, and can be estimated as follows:

$$P_r = \rho_w g y + \rho_s g Z_{BSR} + P_o \quad (13)$$

where ρ_w is water density (kg/m^3); g is standard gravity constant (9.8 m/s^2); ρ_s is sediment density above BSRs (kg/m^3); P_o is atmospheric pressure (psi). The seafloor of the Makassar Strait is primarily composed of mud (Kuhnt et al. 2011). Consequently, the water density near the seafloor was assumed to be $1,025 \text{ kg/m}^3$, while the bulk sediment density was estimated at $1,700 \text{ kg/m}^3$ (Graw et al. 2021). In the study area, an average high geothermal gradient ($73 \text{ }^\circ\text{C/km}$) based on BSRs-controlled

heat flow estimation was proposed by Dirgantara et al. (2025, *in press*). Assuming a linear geothermal gradient, this value is extrapolated to derive the temperature at reservoir depth.

Monte Carlo simulation is employed for probabilistic estimation to address uncertainties in each input parameter. A similar methodology has been applied in assessing methane hydrate potentials in various regions such as the Gulf of Mexico (Majumdar and Cook 2018) and the fold-and-thrust belts off SW Taiwan (Lin 2011; Dirgantara et al. 2020a). Each parameter's statistical distribution is defined within a range of possible values used in the stochastic calculations. Percentiles such as P10, P50, and P90 are utilized to represent the probabilities of specific reservoir properties falling within a given range of forecast uncertainty. The P50 percentile is chosen as the most probable outcome in this study.

Results

Seafloor morphology

Comprehensive seismic interpretation reveals the water depth of the study area between 400 and 2,050 m (Fig. 4) covering the continental slope, continental rise, and abyssal plain of the SMB. The abyssal plain dominates the morphology with minimal surface erosion. On the northwest side, there is a gradual shallowing towards the slope of the Paternoster Platform, while the eastern part

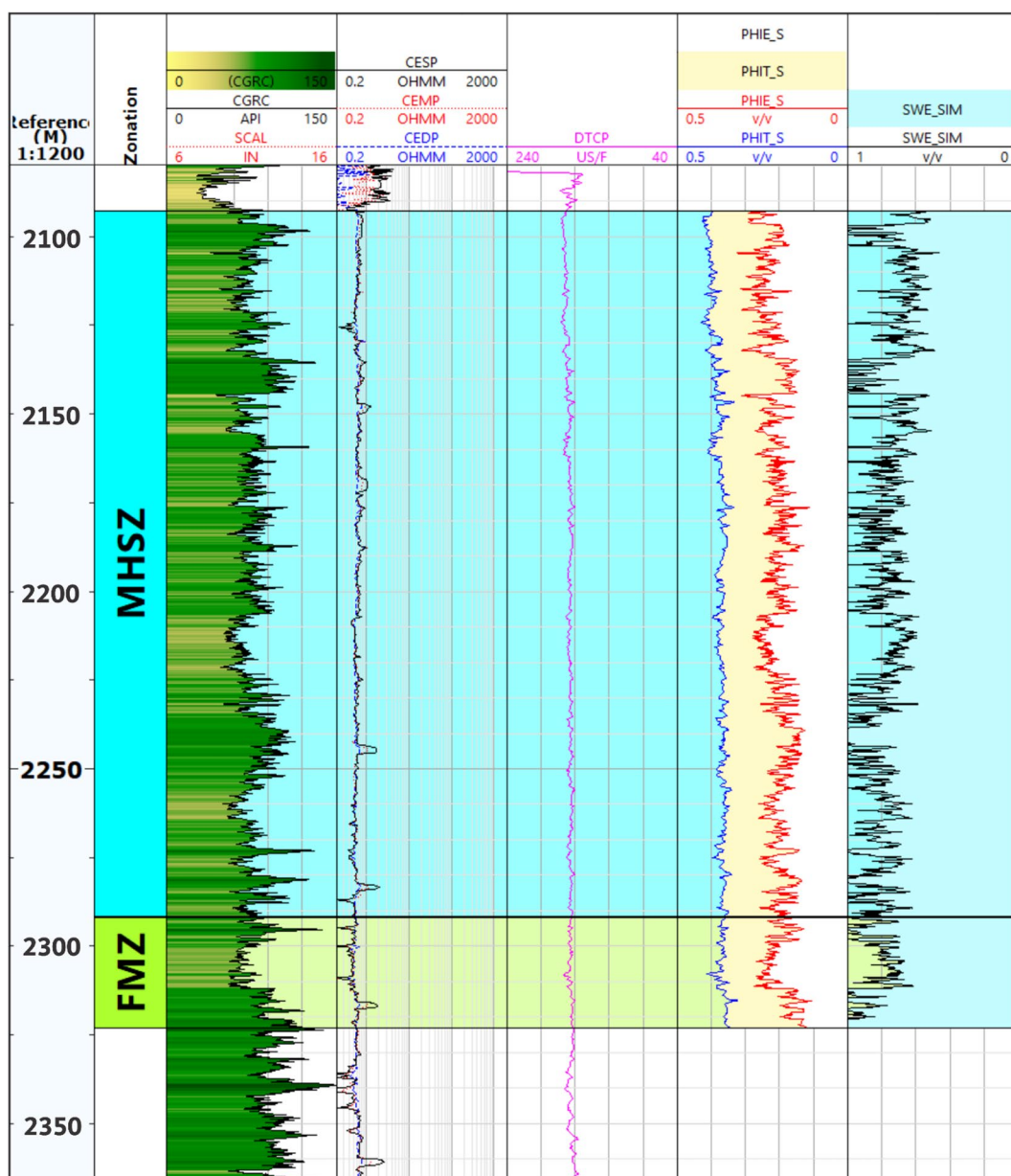


Fig. 8 The interpretation of methane hydrates and free methane zones from the petrophysical data of the Sultan well is based on three available logs: gamma-ray, resistivity, and sonic logs. Refer to Fig. 2 for location. MHSZ = methane hydrate stability zone. FMZ = free methane zone

gradually becomes shallower towards the western offshore slope of Southern Sulawesi. These slopes exhibit characteristics such as sediment gravity redeposition and

erosional sediments within channel-fan systems (Kuhnt et al. 2011). In the abyssal plain, the presence of numerous pockmarks, indicative of active fluid seepages, has been observed (Decker et al. 2004; Courel et al. 2011). A narrow sill, coined as Labani Channel, with depths ranging from 1,000 to 1,900 m, links the SMB to the NMB (Figs. 2, 4).

Table 1 Parameter ranges for defining gas compressibility and gas formation volume factor (FVF) for free methane below BSRs

Reservoir depth (m)	Reservoir pressure (psi)	Reservoir temperature ($^{\circ}$ Rankine)	Gas compressibility	Gas FVF
2321	3437	522.7	0.810	0.00348

Table 2 Reservoir and petrophysical parameters used in defining the first order volumetric estimation for methane hydrate above BSRs

Parameter	Type of distribution	Range
Area (km^2)	Triangular	0:7,335:14,670
Thickness (m)	Log normal	$\bar{x}=198, \sigma=10$
Net-to-gross	Log normal	$P_{10}=0.24, P_{90}=0.36$
Porosity	Log normal	$P_{10}=0.16, P_{90}=0.26$
Hydrate saturation	Log normal	$P_{10}=0.11, P_{90}=0.33$
Volume ratio	Uniform	164
Cage occupancy	Triangular	0:9:0.95:1.0

Table 3 Reservoir and petrophysical parameters used in defining the first-order volumetric estimation for free methane below BSRs

Parameter	Type of distribution	Range
Area (km^2)	Triangular	0:7,335:14,670
Thickness (m)	Log normal	$\bar{x}=31, \sigma=1.00$
Net-to-gross	Log normal	$P_{10}=0.24, P_{90}=0.36$
Porosity	Log normal	$P_{10}=0.15, P_{90}=0.24$
Methane saturation	Log normal	$P_{10}=0.10, P_{90}=0.18$
$1/B_g$	Uniform	286.89

Occurrence of BSRs

Around 78% of seismic lines in this study exhibit BSRs, which are observed across the SMB, intersecting inclined sedimentary reflections with opposite polarity compared to seafloor reflection (Fig. 5). While most follow a parallel pattern to the seafloor, some show variations in depth within the basin (Fig. 6). BSRs amplitudes vary widely, with most displaying high-amplitude reversed-phase reflections while others show low amplitude signatures. Some BSRs form continuous patterns easily seen in seismic profiles, while others do not follow this typical pattern. The BSRs are concentrated in topographic highs, in basin depocenter, and along the basin margin. The depth of BSRs ranges from 100 to 900 m below seafloor (Fig. 7).

Reservoir parameters

The characteristics of BSRs divide potential reservoirs into methane hydrate reservoirs above BSRs and free methane reservoirs below BSRs. The coverage closure for both types of reservoirs assumes the continuous extension of BSRs across the entire area, estimating an approximate area of 14,670 km^2 . This study, utilizing drilling data from well Sultan, reports a consistent thickness of 198 m for methane hydrate reservoirs, located from 2,092 to 2,290 m depth. Similarly, the free methane reservoir is assumed to have a constant thickness, with its upper

boundary at the base of the methane hydrate reservoir and its lower boundary identified by deflections in sonic and deep resistivity logs at 161.27 $\mu\text{s}/\text{ft}$ and 0.57 $\Omega\cdot\text{m}$, respectively (Fig. 8). This defines an average thickness of 31 m for the free methane reservoir below the MHSZ, spanning depths from 2,290 to 2,321 m.

Based on the Wyllie time-average relationship, estimated total and effective porosities within the MHSZ suggest an average value of 37% and 21%, respectively. Using a similar approach, the derived mean total porosity and effective porosity in the FMZ are 36% and 19%, respectively. Water resistivity determination is derived from Simandoux relationship with water resistivity values of 0.0152 $\Omega\cdot\text{m}$ for methane hydrate reservoir and 0.0158 $\Omega\cdot\text{m}$ for free methane reservoir. Utilizing Eq. 5, the water saturation within methane hydrate reservoirs and free methane reservoirs yields estimated percentages of 78% and 86%, correspondingly. This results in an approximate methane hydrate saturation of 22% and a free methane saturation of about 14%.

The gas formation volume factor and gas compressibility are determined based on the average depth and predicted reservoir temperature of each reservoir. Utilizing the time-to-depth conversion (Eq. 12), a linear geothermal gradient (Dirgantara et al. 2025, *in press*), and assuming a constant overburden pressure (Eq. 13), the average values for the depth, temperature, and pressure of the free methane reservoir are estimated at 2321 m, 522 °R, and 3,437 psi, respectively. Since the drilling report of well Sultan suggests that methane is the predominant gas, its critical pressure and temperature are assumed to be 4.60 MPa and 190.6 K, respectively (Elliot and Lira 2012). These inputs are then used in Eq. 11 to calculate the Z values of 0.810. Subsequently, incorporating each reservoir's pressure and temperature conditions into Eq. 10 yields estimated B_g values of 0.003486. The reciprocal of B_g values ($1/B_g$) can be derived as 286.89. Summary regarding free methane reservoir parameters is presented in Table 1.

Reservoir parameters are defined by a range of possible values applied in stochastic models, determined through Monte Carlo stochastic simulations performed over 10,000,000 iterations. These simulations incorporate random variations within the thresholds of the input parameters (Tables 2, 3). For initial estimates, this approach is highly effective in addressing significant uncertainties. The range of uncertainty in potential volumes is represented by a probability distribution. Based on the number of uncertainties and the defined ranges for each parameter, the Monte Carlo method produces a distribution of possible outcome values. A similar methodology has been employed for volumetric estimations in the Nankai

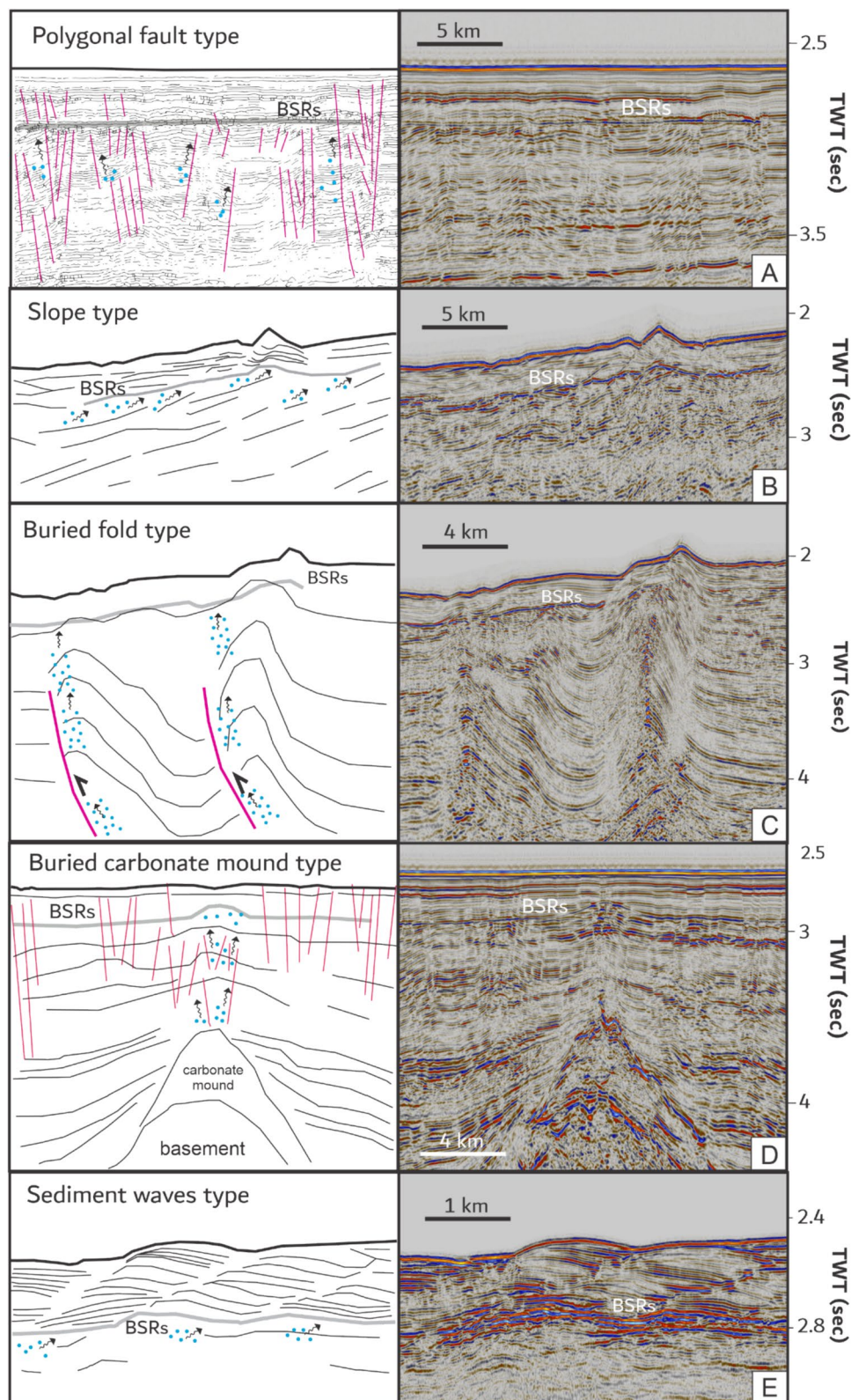


Fig. 9 Simplified schematic illustration of five BSRs types (left boxes) and corresponding uninterpreted seismic (right boxes) in the study area. Blue dots indicate possible migrating methane gas, while red lines are faults. Refer to Fig. 2 for location

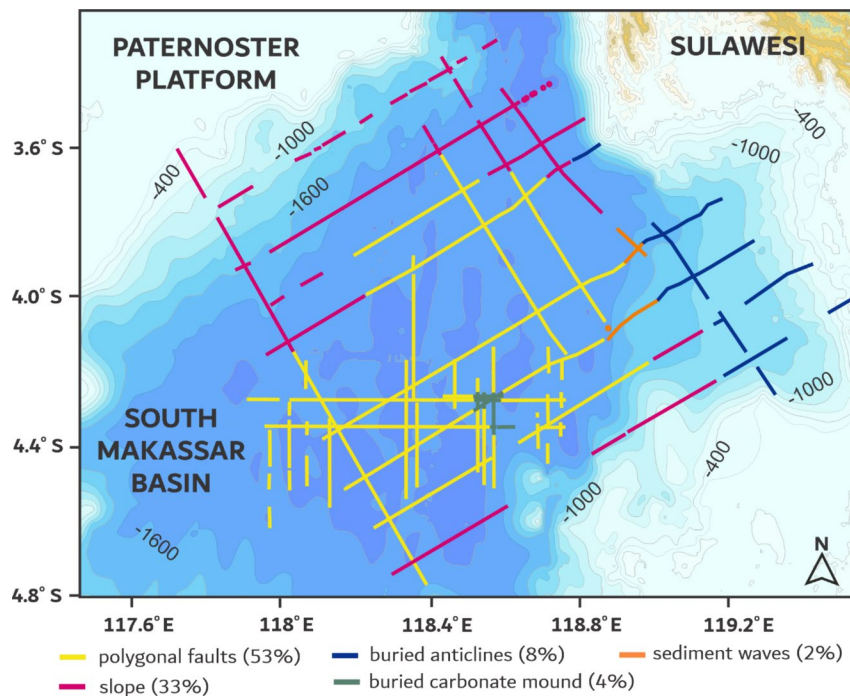


Fig. 10 The spatial distribution of each play type and their qualitative distribution shown in percentage. The dominant play type in the study region is characterized by polygonal fault-related BSRs, while the sediment waves type is the least prevalent

Trough (Fujii et al. 2009) and SW Taiwan (Lin 2011; Dirgantara et al. 2020a).

Discussion

Nature of BSRs

The characteristics of BSRs in this study showcases varying amplitudes, with most displaying high-amplitude reversed-phase reflections while others show low amplitude signatures. BSRs are assumed to represent the phase boundary of methane hydrate stability, with the reversed polarity indicating higher acoustic impedance from methane hydrates compared to free methane accumulation (Dirgantara et al. 2023). Some BSRs form continuous patterns easily discernible in seismic profiles, but others do not follow this typical pattern. While the presence of BSRs often indicates the likely presence of methane hydrates, the opposite is not always true. Studies from the Gulf of Mexico (Dai et al. 2004; Hardage and Roberts 2006) and offshore SW Taiwan (Lin 2011; Dirgantara et al. 2020a, b) reveal that methane hydrates can exist without accompanying BSRs. In the SMB, proven methane hydrates samples have been inferred from the past drilling and coring activities (Bacheller III et al. 2011; de Man et al. 2011; Courel et al. 2011). This suggests that methane hydrates may be present even in areas where the BSRs response is relatively weak or absent.

Additionally, signs suggesting that BSRs are linked to either free methane or methane hydrates include: (1) evident intensified reflections beneath BSRs, indicating the presence of trapped free methane beneath the MHSZ; (2) blanking reflections above BSRs, signifying the existence of methane hydrates; (3) BSRs aligning with areas of fluid venting associated with hydrocarbon migration observed on the seafloor (e.g., Derrick et al. 2004; Courel et al. 2011; Kuhnt et al. 2011). The locations of these discoveries correspond with the distribution map of BSRs, suggesting the likely presence of methane hydrate and free methane systems in the study region.

Play types

Figure 5 shows a characteristic BSR and its associated features in the study area. Based on the relationship of BSRs to seafloor topography and structural features on seismic data, 5 play types are introduced: polygonal fault-associated BSRs, slope-associated BSRs, buried fold-associated BSRs, buried carbonate-associated BSRs, sediment waves-associated BSRs (Fig. 9). Spatially, these types showcase varying degrees of BSRs length: 998 km (53%), 619 km (33%), 144 km (8%), 68 km (4%), and 43 km (2%), respectively (Fig. 9). They are predominantly situated beneath topographic highs and basin depocenter. These play types indicate that the MHSZ persists regardless of variations in bathymetry and subsurface structures.

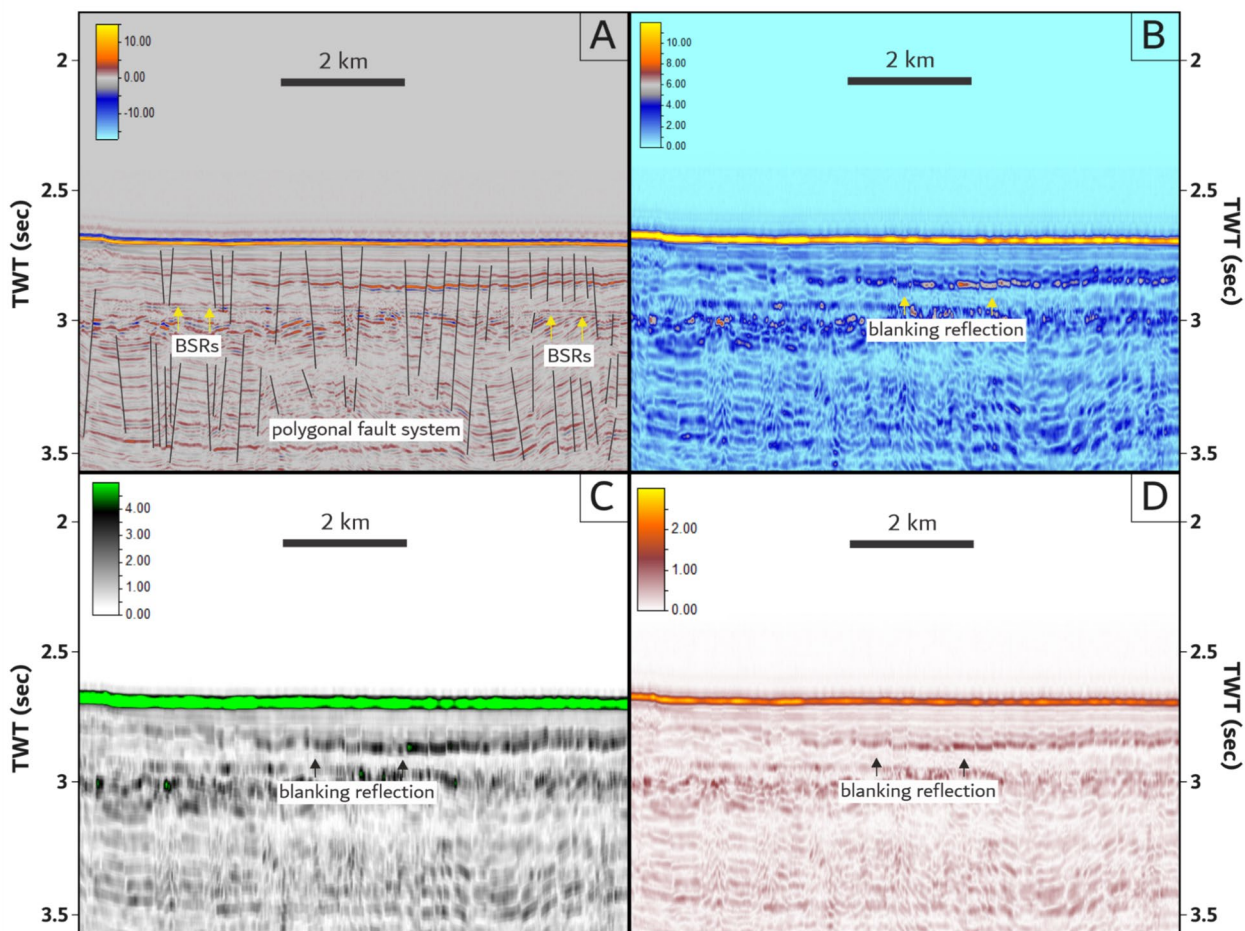


Fig. 11 Comparison of conventional seismic profile (**A**) and various seismic attributes (**B** envelope; **C** RMS amplitude; **D** sweetness) for polygonal fault play type. Distinct blanking zone above BSRs suggesting the presence of methane hydrates. In all attribute profiles, BSRs horizon is characterized by relatively low amplitudes. Refer to Fig. 2 for location

Play type 1: polygonal faults-related BSRs

Pervasive distribution of polygonal fault systems is present in the western, central, and southern parts of the SMB (Fig. 10), mainly in the basin interior. Among the 5 play types, this type exhibits the broadest spatial distribution. These systems are dominated by fault system characterized by the presence of numerous small normal faults that are organized in a polygonal pattern (Fig. 9A). The faults are prominent cutting through shallow overburden sediments with maximum extension down to 5,000 ms (two-way time). Most faults propagate through the entire overburden section, without any preferred apparent dip direction (de Man et al. 2011). Armandita et al. (2015) suggested that the faults cut through Late Miocene to Pleistocene post-rift sediments, including the giant block of mass transport complex near Paternoster Platform. This type of polygonal faulting pattern has been widely described in fine-grained hemipelagic sediments,

and the genesis of polygonal fault system has been attributed to several mechanisms, including gravity collapse, density inversion, syneresis, and compactional loading (Cartwright et al. 2003; Xia et al. 2022). Assuming an average interval velocity of 2,000 m/s, fault offsets range from 5 to 24 m.

In some parts of the area, interpreting the presence of BSRs in this play type poses difficulty due to the parallel alignment of stratal reflections with the BSRs, making differentiation between the two challenging. However, the absence of vertical offset in BSRs compared to faulted reflections aids in their detection. Since most of the polygonal faults intersect the BSRs (e.g., Fig. 6), these suggest how the faults can significantly affect the formation of methane hydrates and free methane. In the Northern Carnarvon Basin, similar faults have been hinted to act as pathways for fluid flow, enhancing the migration of fluids and the formation of methane hydrates (Zeng et al. 2022).

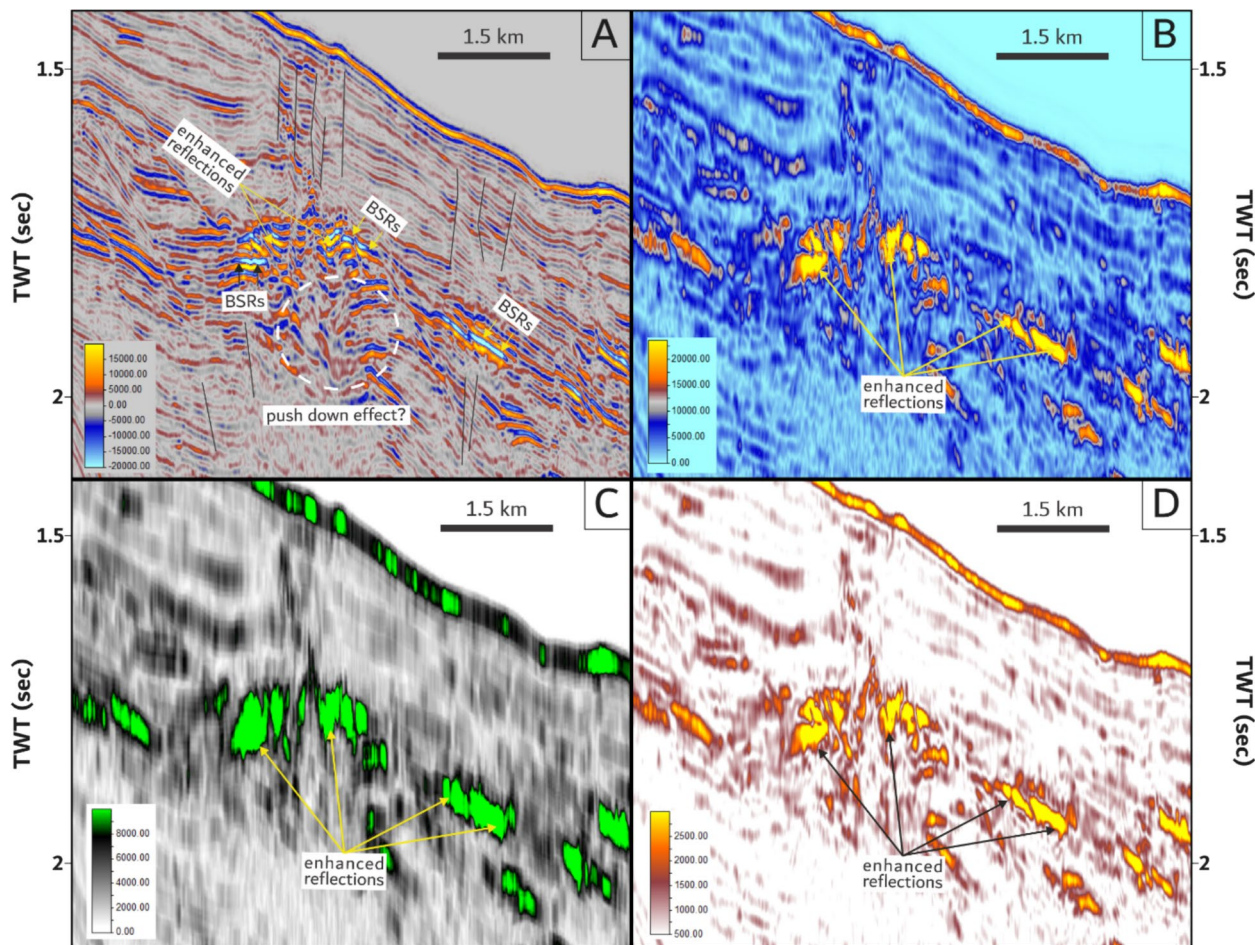


Fig. 12 In slope play type, enhanced reflection is seen in conventional seismic section (**A**), envelope attribute (**B**), RMS amplitude attribute (**C**), and sweetness attributes (**D**) below BSRs, possibly related to methane charging strata. Refer to Fig. 2 for location

In the South China Sea, presence of polygonal faults increases the permeability of fine-grained sediments, facilitating efficient fluid flow and methane hydrate formation (Zhang et al. 2022). Within SMB, polygonal faults function as conduits for the migration of deeply seated thermogenic methane. Furthermore, de Man et al. (2011) observed that the presence of gas chimneys in the area is likely attributed to the concentration of deeply seated gas along fault lines, subsequently ascending as it exceeds the fracture gradient. Seismic attributes of this type exhibit distinct characters with conspicuous blanking reflection above BSRs, suggesting pervasive distribution of methane hydrates (Fig. 11).

Play type 2: slope-related BSRs

Slope-related BSRs develop along the edges of the basin, primarily in the northern and northwestern parts of the SMB. Based on seismic profiles, the dip angle of inclined beds in the basin margin is higher than that in the basin interior. BSRs can be seen in areas where the seafloor topography ascends from relatively flat basin to sloping terrain, with a minimum gradient of 6°. There are two distinct types of BSRs governing this play: (1) BSRs cutting tilted stratal reflections (Fig. 9B); (2) BSRs that are subparallel to tilted reflections (Fig. 12), with the latter being the more predominant group of BSRs. The presence of BSR in this type was clearly observed in the original seismic section characterized by high-amplitude polarity reversal relative to the seafloor. The use of envelope, RMS amplitude, and sweetness attributes enhanced the

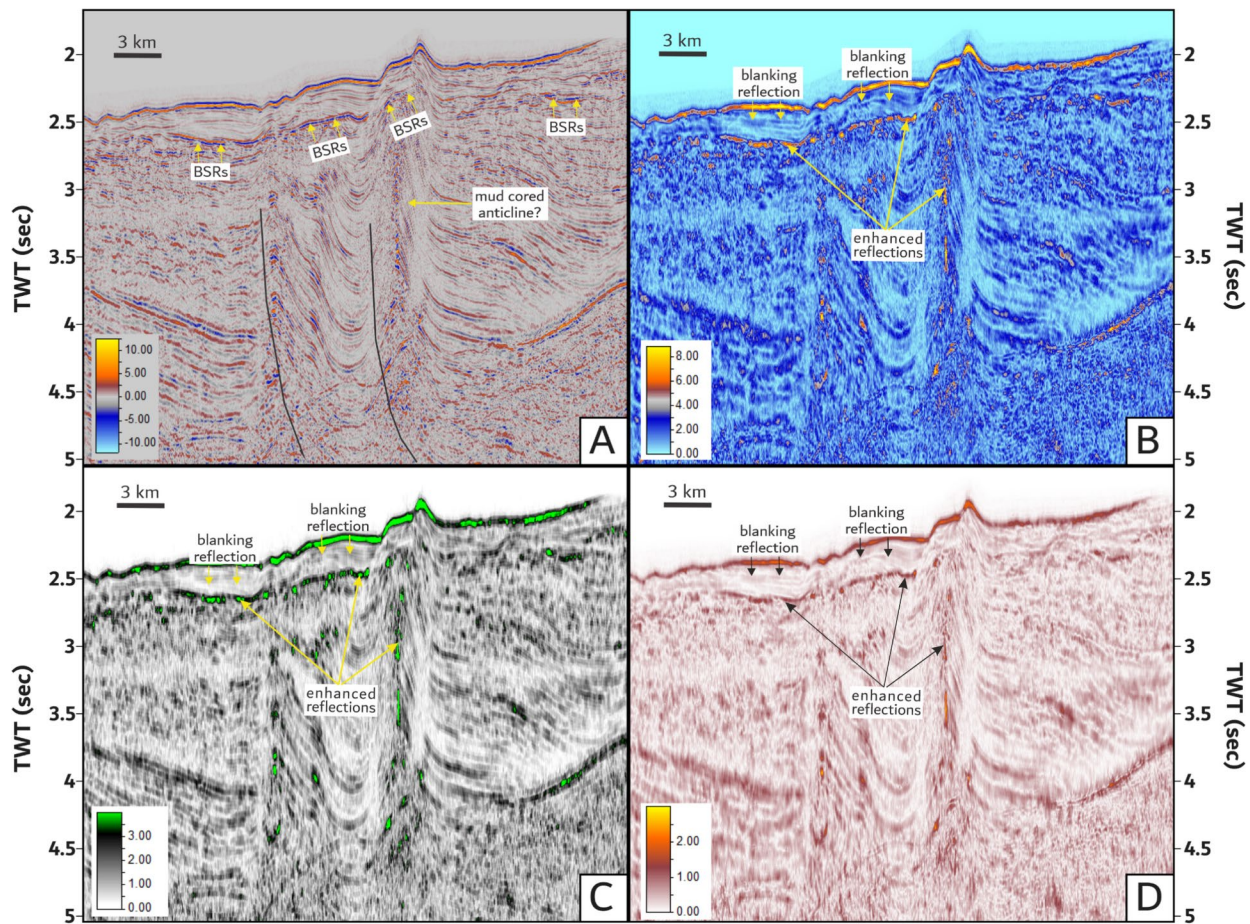


Fig. 13 In the conventional seismic section of buried anticline play type (**A**), BSRs are seen to cross both stratal reflection above the buried fold and its limbs. Although enhanced reflection below BSRs are not always available, discernible blanking reflections above BSRs are available in all seismic sections, including in envelope (**B**), RMS amplitude (**C**), and sweetness (**D**) attributes. Refer to Fig. 2 for location

amplitude associated with free methane above and below BSRs. Push down effect is also seen where the presence of gas in the subsurface causes a delay in the travel time of seismic waves and a decrease in amplitude in the seismic section (Fig. 12). This effect is likely related to the upward migration of deep-seated gas.

Play type 3: buried fold-related BSRs

This play type is defined by the development of BSRs within compressional folds in the eastern SMB (Fig. 10). These structures are comparable to WSFB, as proposed by Nur'Aini et al. (2005), in the eastern NMB region. However, these buried folds show no geomorphic surface expression, implying a more recent developmental phase in contrast to the corresponding structures in the NMB.

BSRs cut across the strata either above the folds or across the limb of folds (Figs. 9C, 13). Enhanced reflections are apparent in all seismic sections, both conventional and attribute sections. Mud-cored anticlines showing internal enhanced reflections indicate that the formation of fold-and-thrust structures in the SMB is strongly influenced by the ascent of mud diapirs carrying deep-seated thermogenic methane. This phenomenon is also observable in any other convergent margin around the world, e.g. northeastern South China Sea (Dirgantara et al. 2020a, b), southern Okinawa Trough (Ning et al. 2009), and northwestern Sea of Okhotsk (Ludmann and Wong 2003). The development of fold-and-thrust structures in the SMB is likely linked to the onset of a compressional tectonic phase in the eastern part of the Makassar Strait

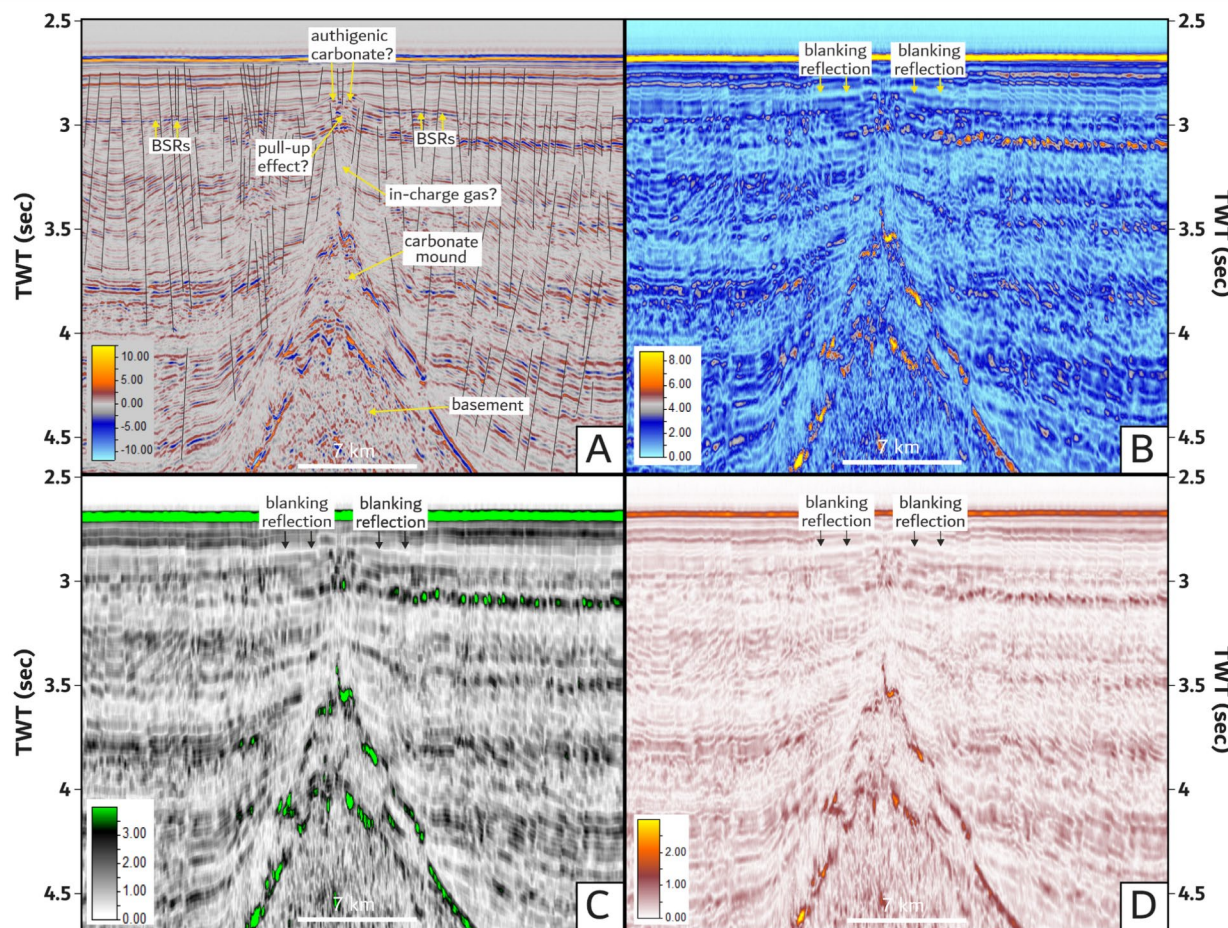


Fig. 14 Buried-carbonate type is characterized by polygonal faults enclosing buried carbonate mound. In conventional seismic (**A**), gas in charge above buried carbonate is seen as low frequency blanking reflection. This reflection, however, is not visible in envelope (**B**), RMS amplitude (**C**), and sweetness (**D**) attributes. Refer to Fig. 2 for location

since the early Pliocene (Fraser et al. 2003; Baillie et al. 2004; Nur A'ini et al. 2005).

Play type 4: buried carbonate-related BSRs

Buried carbonate BSRs are found adjacent to polygonal fault structures (Figs. 9D, 10), resembling those within the polygonal fault system but situated above buried carbonate mounds (Fig. 14). Conjugate pairs of normal faults identified in 3D seismic data converge downward just above the carbonate mound (de Man et al. 2011). The presence of upward migrating gas above buried carbonate manifests as low-frequency blanking reflections, although not consistently visible across all seismic attributes. Moreover, enhanced reflections below BSRs are also

not consistently observable. Authigenic carbonate formation at shallower depth is evidenced by elevated high-amplitude seismic signals between BSRs and the seafloor. This carbonate formed in situ through the interaction of methane released from hydrates with seawater, leading to the formation of calcium carbonate via reactions with bicarbonate and calcium ions (Callow et al. 2021). The pull-up effect attributed to authigenic carbonate results from its higher density and elastic properties compared to the surrounding sediment, causing an increase in seismic velocity and shorter travel time (Fig. 14).

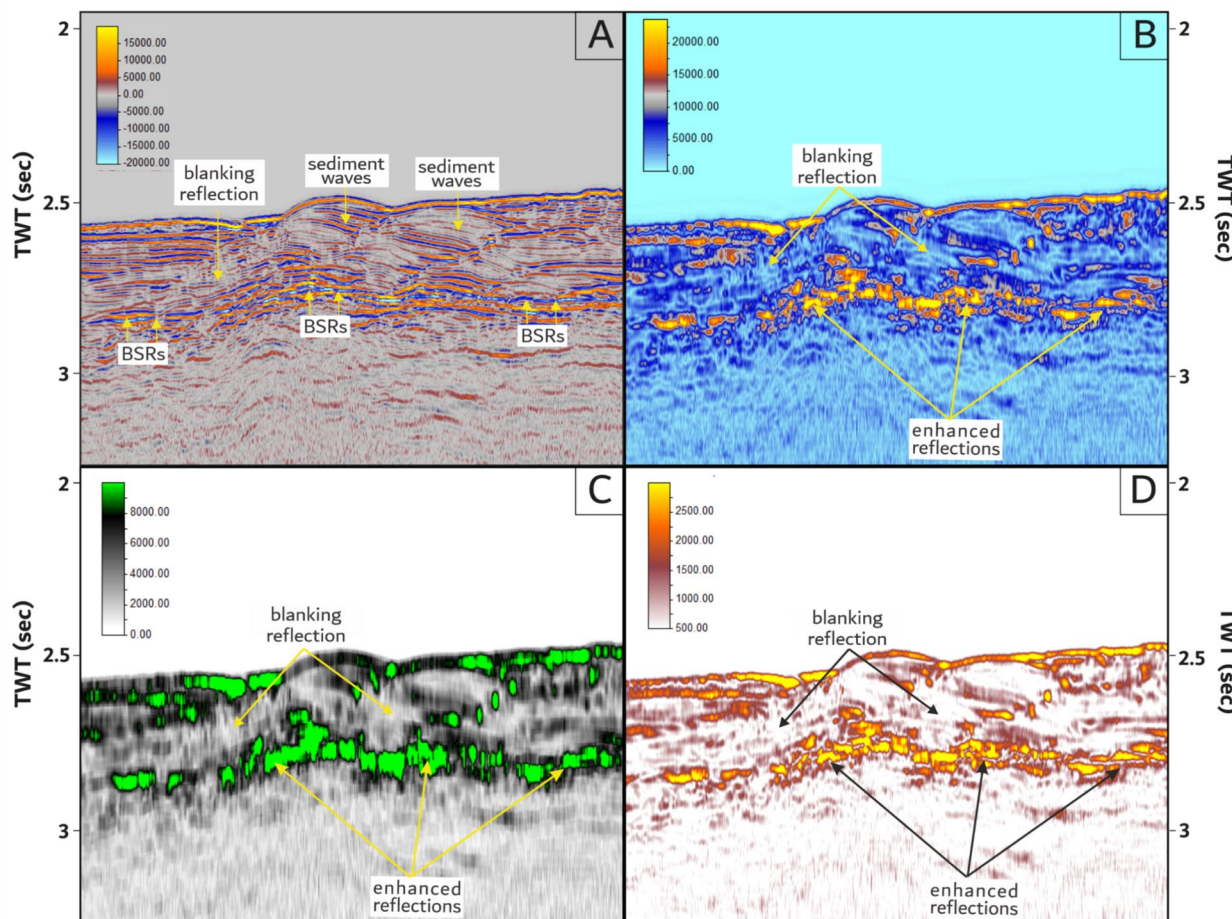


Fig. 15 Due to the presence of charging methane beneath BSRs, enhanced reflections can be seen in standard seismic (**A**), envelope (**B**), RMS amplitude (**C**), and sweetness (**D**) attributes within sediment wave types. On the other hand, blanking reflection is partially visible above BSRs. Refer to Fig. 2 for location

Play type 5: sediment waves-related BSRs

Localized distribution of sediment waves is distinguishable between slope type and polygonal fault type (Figs. 9E, 10). Sediment waves are generated beneath currents flowing across the seabed, in the form of either downslope-flowing turbidity currents or along slope-flowing bottom currents (Wynn and Stow 2002). Enhanced reflection and partial blanking areas below and above BSRs, respectively, are discernible across all seismic attributes, indicating the presence of charged methane layers beneath methane hydrates (Fig. 15). In the South China Sea, sediment waves have been suggested as a prominent reservoir for methane hydrates (Bai et al. 2019).

Potential origin of methane

This study postulates three theories explaining the source of methane in the SMB. The first suggests that methane hydrates form on-site from degradation of organic carbon found in sediment within the MHSZ (e.g., Claypool and Kaplan 1974) or biogenic origin. Conversely, the second theory proposes that methane hydrates originate from upward-moving fluids containing light hydrocarbons (e.g., Hyndman and Davis 1992) or thermogenic origin. Alternatively, methane hydrates can be re-concentrated through "hydrate recycling", wherein methane hydrates reform from the up-flow of dissociation methane released from existing methane hydrates when the

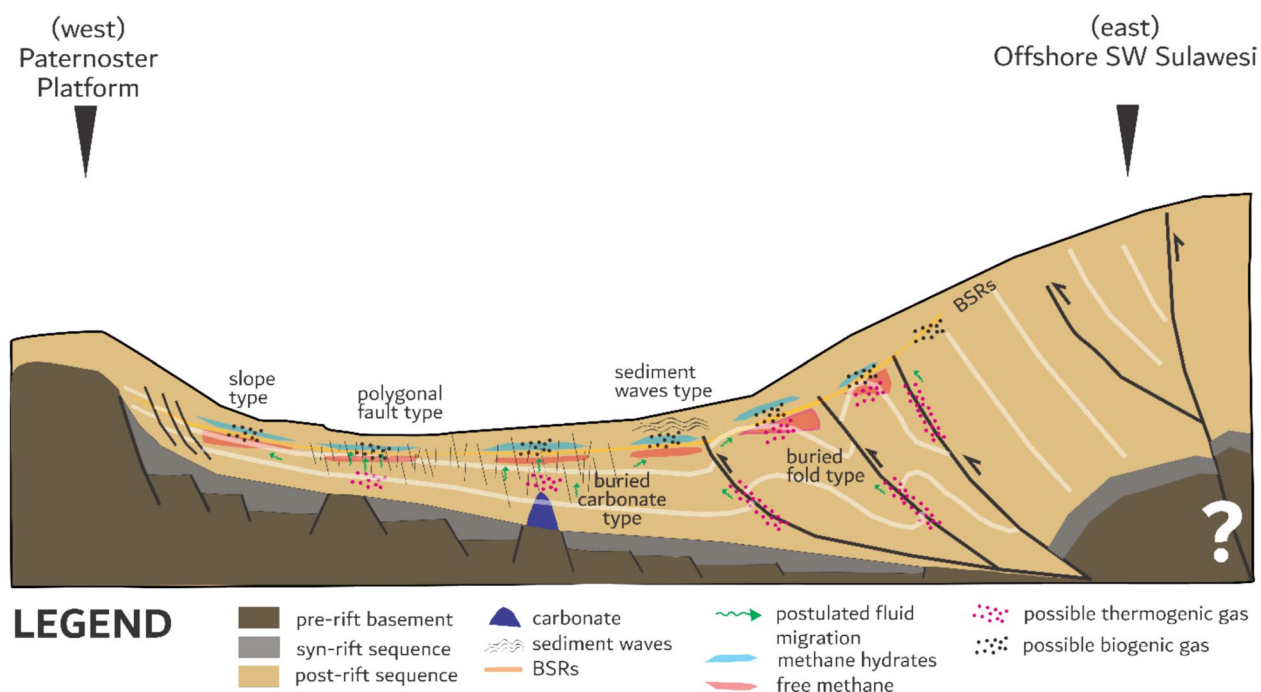


Fig. 16 A schematic diagram summarizing the methane hydrate and related free methane systems in the South Makassar Basin. Note that the figure is not to scale

base of the MHSZ changes due to tectonic uplift or rift-ing processes (Dickens and Forswall 2009).

While direct geochemical measurements at the depth of MHSZ and FMZ are lacking in this study, the drilling report from well Sultan suggests that based on Rock-Eval pyrolysis conducted at the depth of the conventional petroleum reservoir target (Oligocene carbonates), the methane gas is associated with type III thermogenic sources. Similar finding has been suggested by Courel et al. (2011) via shallow methane-hydrates coring within the pockmarks of the SMB. Compositional analysis report from well Sultan suggests dominant gas composition of methane between 87%–98%. Another possibility for the methane source is biogenic origin. Decker et al. (2004), based on carbon and hydrogen isotopes, proposed methane of bacterial origin in the SMB. In the NMB, both biogenic and thermogenic methane origins have been suggested in the Miocene–Pliocene reservoirs

(Satyana et al. 2007). Based on isotope geochemistry study, Sassen and Curiale (2006) argued that the source of methane and ethane found in nodular methane hydrate cores within the NMB is likely microbial in nature. Given the relatively shallow average depth of BSRs, this study does not rule out the possibility of mixing thermogenic–biogenic methane sources in the SMB, particularly in play types where faults are predominant, such as polygonal fault-related BSRs, buried fold-associated BSRs, and buried carbonate-related BSRs (Fig. 16).

Volumetric estimation

According to Monte Carlo simulation, the estimated volume of in-place methane in the study area is ~ 105 TCF (Fig. 17). Methane hydrate prospects above BSRs potentially hold the most significant volumes of 88 TCF, whereas free methane below BSRs exhibits volumetric potentials of 17 TCF. This study derives the

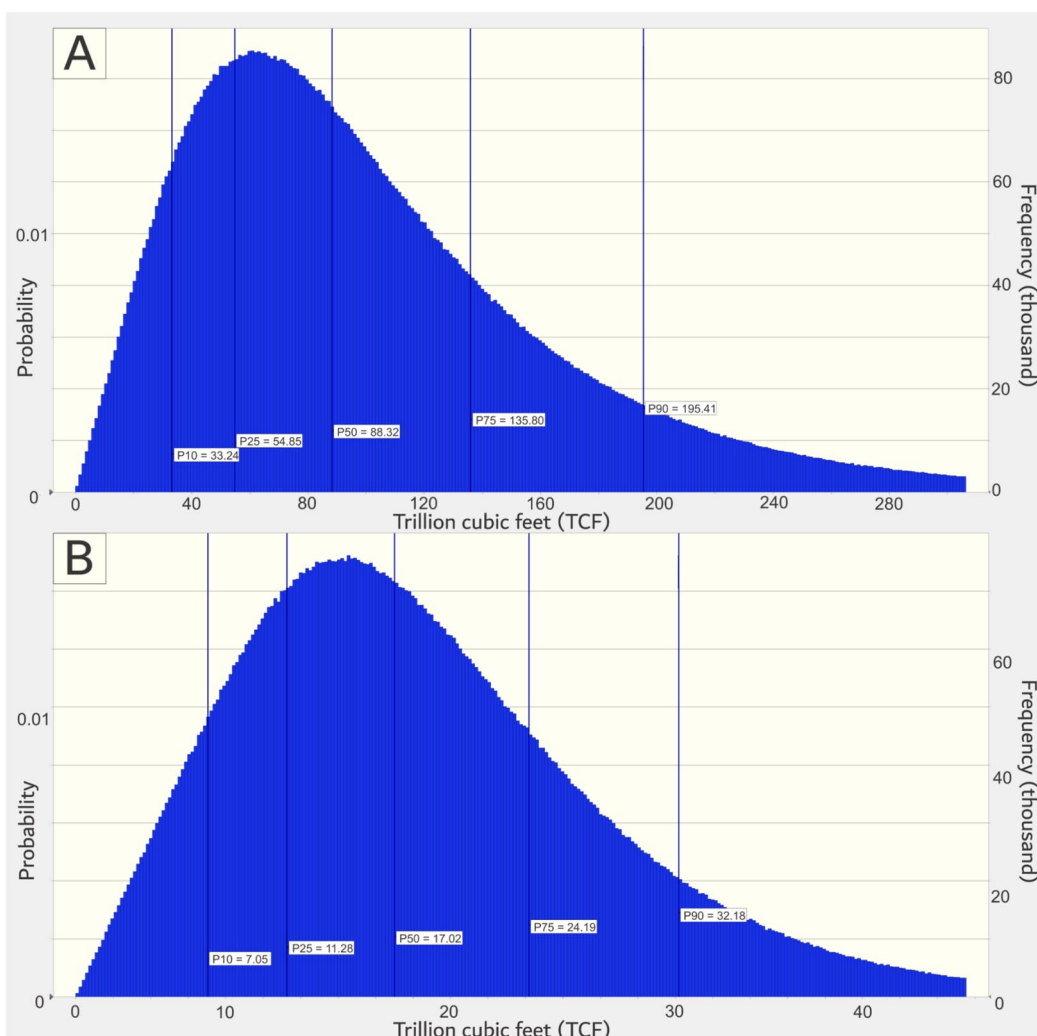


Fig. 17 Monte Carlo probabilistic estimation of in-place gas volumes for **A** methane-hydrates reservoirs above BSRs and **B** free methane reservoirs below BSRs

petrophysical parameters and thickness estimation from well Sultan; and the area from seismically interpreted BSRs distribution. The volumetric estimation is not free of limitation. The distribution of methane hydrates is sensitive to pore pressure (Xu and Germanovich 2006), geothermal gradient (Grevenmeyer and Villinger 2001), sediment thermal conductivity (Waite et al. 2007), sediment grain size and mineralogy (Wood et al. 2002), effective stress (Hyodo et al. 2017), pore water salinity (You et al. 2015), gas solubility (You et al. 2019) and pore water availability (Gorntz and Fung 1994). Relying solely on the data from a single well log across an expansive area spanning 14,670 km² may introduce potential inaccuracies in the estimation of petrophysical properties. Assumptions related to petrophysical derivation may not satisfy the actual subsurface lithology. Furthermore, since this

study operates under the premise that BSRs uniformly extend throughout the entire study area, it is imperative to acknowledge and anticipate uncertainties in the derived estimates. Nevertheless, this study presents a first-order estimate of methane-bearing zones in the SMB, contributing to the future deep-sea hydrocarbon exploration in offshore southern Makassar Strait.

Conclusions

This research provides a novel assessment of methane hydrates and their associated free methane systems in the SMB, as depicted in the schematic diagram of Fig. 16. Based on seismic interpretation and attributes, five distinct play types of BSRs have been identified: polygonal faults, slope features, buried folds, buried

carbonate mounds, and sediment waves. The salient characteristics of BSRs in this region include:

1. Predominantly located beneath elevated topographic features and within basin depocenters.
2. Typically exhibiting a series of high-amplitude dipping reflectors beneath BSRs.
3. The distribution of BSRs is not consistently continuous and does not always align parallel to the seafloor.
4. The presence of blanking reflections above BSRs varies significantly.

These observations suggest a preferential accumulation of methane hydrates beneath structural highs and basin depocenters, likely attributed to the upward and lateral migration of buoyancy-driven, methane-bearing fluids towards. By analyzing seismic attributes, seismic amplitude characteristics, reflection strength, and depth of the BSRs, hydrocarbon prospects can be categorized into methane hydrate compartments located below BSRs and free methane compartments located above BSRs. Petrophysical analysis and Monte Carlo simulations indicate that the prospects appear to hold an estimated 105 TCF of total gas volume across a study area spanning 14,670 km². These results offer a comprehensive framework for understanding methane hydrate dynamics in the SMB, advancing both scientific knowledge and resource exploration efforts in the area.

Acknowledgements

This study is part of first author's postdoctoral research work at the Research Center for Geological Resources, National Research and Innovation Agency (BRIN) Indonesia. We acknowledge the Ministry of Energy and Mineral Resources of Indonesia and Data and Information Center (Pusdatin-ESDM) for the data permission and use. The constructive feedback and recommendations provided by two anonymous reviewers and the editor are deeply appreciated.

Author contributions

FD: conceived and design the analysis, contributed to data analysis, performed the analysis, wrote and edited the paper, created tables and figures. SS: collected the data, edited the paper. MASL: collected the data, contributed to data analysis, created figures, wrote the paper. YAS: contributed to data analysis, created figures, wrote the paper.

Funding

Not applicable.

Availability of data and materials

The seismic reflection data and well reports belong to the Ministry of Energy and Mineral Resources of Indonesia, and available for public via its Data and Information Center (Pusdatin-ESDM).

Declarations

Competing interests

The authors declare that they have no competing interests.

Received: 10 April 2024 Accepted: 5 January 2025

Published online: 04 February 2025

References

- Armandita C, Morley CK, Rowell P (2015) Origin, structural geometry, and development of a giant coherent slide: the South Makassar Strait mass transport complex. *Geosphere* 11(2):376–403
- Bacheller III J, Buck SP, Cahyono AB, Polis SR, Helsing CE, Zulfitriadi Z, de Man EM, Hillock PM, Ruf AS, Toxey JK (2011) Early deepwater drilling results from a new exploration play, offshore West Sulawesi, Indonesia. In: Proceedings Indonesian Petroleum Association 35th Annual Convention.
- Bahar A, Santoso D, Hakiki F, Widiyantoro S, Surachman Y (2006) Seismic identification and characterization of gas hydrates in Central Sunda margin - Indonesia. In: Proceedings of the 8th SEGJ international symposium, Japan
- Bai C, Zhang G, Lu J, Liang J, Yang Z, Yan W, Zhu D, Tian Y (2019) Deep-water sediment waves as a special gas hydrate reservoirs in the Northeastern South China Sea. *Mar Pet Geol* 101:476–485
- Baillie P, Darman H, Fraser TH (2004) Deformation of Cenozoic basins of Borneo and West Sulawesi. In: Proceedings of Indonesian Petroleum Association 28th Annual Convention
- Callow B, Bull JM, Provenzano G, Böttner C, Birinc H, Robinson AH, Henstock TJ, Minshull TA, Bayrakci G, Lichtschlag A, Roche B, Yilo N, Gehrmann R, Karstens J, Falcon-Suarez IH, Berndt C (2021) Seismic chimney characterisation in the North Sea – implications for pockmark formation and shallow gas migration. *Mar Pet Geol* 133:105301
- Cartwright JA, James DMD, Bolton AJ (2003) The genesis of polygonal fault systems: A review. *Geol Soc London Spec Public* 216:223–243
- Chen Q, Sidney S (1997) Seismic attribute technology for reservoir forecasting and monitoring. *Lead Edge* 16(5):445–448
- Chopra NN (1985) Gas hydrates - an unconventional trap in the forearc regions of Andaman offshore. *ONGC Bull* 22(1):41–54
- Clairmont R, Bedle H, Marfurt K, Wang Y (2021) Seismic attribute analyses and attenuation applications for detecting gas hydrate presence. *Geosciences* 11(11):450
- Claypool GE, Kaplan LR (1974) The origin and distribution of methane in marine sediments. In: Kaplan LR (Eds) *Natural gases in marine sediments*. Plenum Press, New York, pp 99–139
- Collett TS, Riedel M, Cochran J, Boswell R, Presley J, Kumar P, Sathe AV, Sethi AK, Lall MV, Sibal V.K, NGHP Expedition 01 Scientists (2008) NGHP Expedition 01. Initial Reports. Directorate General of Hydrocarbons, NOIDA and Ministry of Petroleum & Natural Gas, India (4).
- Courel R, Begg P, Kim M, Kokoh L, Nasif K (2011) Heat Flow measurements and mapping from BSR to constrain the evaluation of the deepwater South Makassar Basin. International Petroleum Technology Conference 14555.
- Dai J, Xu H, Snyder F, Dutta N (2004) Detection and estimation of gas hydrates using rock physics and seismic inversion: Examples from the northern deepwater Gulf of Mexico. *Lead Edge* 23(1):60–66
- Davies IC (1990) Geological and exploration review of the Tomori PSC, Eastern Indonesia, In: Proceedings Indonesian Petroleum Association 19th Annual Convention
- Decker J, Teas PA, Curiale J, Johnson EC, Elizabeth EAE, Orange DL (2004) Multibeam exploration in the Makassar Strait. In: Proceedings Indonesian Petroleum Association 28th Annual Convention
- Delisle G, Beiersdorf H, Neben S, Steinmann D (1998) The geothermal field of the North Sulawesi accretionary wedge and a model on BSR migration in unstable depositional environments. *Geol Soc London Spec Public* 137:267–274

- Dewan JT (1983) Essentials of modern open-hole log interpretation. Penn Well Books, Oklahoma
- Dickens GR, Forswall C (2009) Methane hydrates, carbon cycling, environmental change. In: Gornitz V (Eds) Encyclopedia of paleoclimatology and ancient environments. Springer, Dordrecht
- Dickens GR, O'Neil JR, Rea DK, Owen RM (1995) Dissociation of oceanic methane hydrate as a cause of the carbon isotope excursion at the end of the Paleocene. *Paleoceanography* 10:965–971
- Dirgantara F, Lin ATS, Liu CS, Lin CC, Chen SC (2020a) Gas-hydrate systems and gas volumetric assessment in the Lower Fangliao Basin, Taiwan accretionary wedge. *J Pet Geol* 43(1):27–48
- Dirgantara F, Chiang HT, Lin ATS, Liu CS, Chen SC (2020b) Depositional influence of submarine channel migration on thermal properties of the Lower Fangliao Basin, offshore southwestern Taiwan. *Marine Geophys Res* 41(1):1–23
- Dirgantara F, Lin ATS, Liu CS (2023) Seismic de-multiple strategy in the submarine slope of Taiwan accretionary wedge. *Explor Geophys* 54(2):117–132
- Dirgantara F, Susilohadi S, Suyanto I, Iskandar MAS (2025) Subsurface thermal properties in the deepwater South Makassar Basin, Indonesia. *J Asian Earth Sci*
- Doust H, Noble RA (2008) Petroleum systems of Indonesia. *Mar Pet Geol* 25:103–129
- Elger J, Berndt C, Rupke L, Krastel S, Gross F, Geissler WH (2018) Submarine slope failures due to pipe structure formation. *Nat Commun* 9:715
- Elliott JR, Lira CT (2012) Introductory chemical engineering thermodynamics. Prentice Hall, New York
- Fraser TH, Jackson BA, Barber PM, Baillie P, Myers K, Darman H (2003) The West Sulawesi fold belt and other new plays within the North Makassar straits – A prospectivity review. In: Proceedings Indonesian Petroleum Association 29th Annual Convention
- Fujii T, Saeki T, Kobayashi T, Inamori T, Hayashi M, Takano O, Takayama T, Kawasaki T, Nagakubo S, Nakamizu M, Yokoi K (2009) Resource assessment of methane hydrate by applying a probabilistic approach in the eastern Nankai Trough, Japan. *J Geogr* 118:814–834
- Garcia-Tigreros F, Leonte M, Ruppel CD, Ruiz-Angulo A, Joung DJ, Young B, Kessler JD (2021) Estimating the impact of seep methane oxidation on ocean pH and dissolved inorganic radiocarbon along the U.S Mid-Atlantic Bight. *J Geophys Res Biogeosciences* 126:e2019
- General Bathymetric Chart of the Oceans (GEBCO) Compilation Group, 2023. GEBCO 2023 Grid. British Oceanographic Data Centre, National Oceanography Centre, NERC, UK.
- Gornitz V, Fung I (1994) Potential distribution of methane hydrates in the world's oceans. *Global Biogeochem Cycles* 8(3):335–347
- Graw JH, Wood WT, Phrampus BJ (2021) Predicting global marine sediment density using the random forest regressor machine learning algorithm. *J Geophys Res Solid Earth* 126:e2020
- Gretemeyer I, Villinger H (2001) Gas hydrates stability and the assessment of heat flow through continental margins. *Geophys J Int* 145:647–660
- Guntoro A (1999) The formation of the Makassar Strait and the separation between SE Kalimantan and SW Sulawesi. *J Asian Earth Sci* 17:79–98
- Hall C, Cloke IR, Nur'aini S, Puspita SD, Calvert SJ, Elders CF (2009) The North Makassar Straits: what lies beneath? *Pet Geosci* 15:147–158
- Hamilton EL (1980) Geoaoustic modeling of the seafloor. *J Acoust Soc Am* 68:1313–1340
- Hardage BA, Roberts HH (2006) Gas hydrate in the Gulf of Mexico: What and where is the seismic target? *Lead Edge* 25(5):566–571
- Hideyat R, Husein S, Surjono SS (2012) Regional depositional model of South Makassar Basin depocenter, Makassar Strait, based on seismic facies. *J SE Asian Appl Geol* 4(1):42–52
- Holdaway KR (2014) Harness oil and gas big data with analytics: Optimize exploration and production with data-driven models. John Wiley & Sons, New Jersey
- Hyndman RD, Davis EE (1992) A mechanism for the formation of methane hydrate and seafloor bottom-simulating reflectors by vertical fluid expulsion. *Jour Geophys Research* 97:7025–7041
- Hyodo M, Wu Y, Nakashima K, Kajiyama S, Nakata Y (2017) Influence of fines content on the mechanical behavior of methane hydrate-bearing sediments. *J Geophys Res Solid Earth* 122:7511–7524
- Jackson BA (2004) Seismic evidence for gas hydrates in the North Makassar Basin, Indonesia. *Pet Geosci*, 10(3):227–238
- Kopp H (2002) BSR occurrence along the Sunda margin: Evidence from seismic data. *Earth Planet Sci Lett* 197:225–235
- Kuhnt W, Holbourn A, Regenberg M, Zuraida R, Abbyoso S, Aquit M, Balmer S, Djajadiredja M, Fraser N, Jeschlitschek H, Kawohl H, Kubner K, Kust M, Capelli EL, Lorenzen J, Masfaraan H, Muller S, Nurdin N, Schröde J, Steen E, Xu J (2011) Variability of the Indonesian Throughflow with the Makassar-Java passage. *Cruise Report Sonne* 217.
- Kumar J, Sain K, Arun KP (2018) Seismic attributes for characterizing gas hydrates: A study from the Mahanadi offshore, India. *Mar Geophys Res* 40:73–86
- Kupecz J, Sayers I, Tognini P, Hilman A, Tanos C, Ariyono, D (2013) New insights into the tectono-stratigraphy evolution of the South Makassar Basin. In: Proceedings Indonesian Petroleum Association 37th Annual Convention
- Kvenvolden KA (1999) Potential effects of gas hydrate on human welfare. *Proc Nat Acad Sci* 96:3420–3426
- Lin CC (2011) Geological controls of gas hydrate occurrences and gas hydrate resource assessment, offshore southwest Taiwan (unpublished). National Central University, Taiwan
- Longley IM (1997) The tectonostratigraphic evolution of SE Asia Petroleum geology of southeast Asia. *Geol Soc London*. <https://doi.org/10.1144/GSL.SP.1997.126.01.19>
- Ludmann T, Wong HK (2003) Characteristics of gas hydrate occurrences associated with mud diapirism and gas escape structures in the northwestern Sea of Okhotsk. *Mar Geol* 201:269–286
- Lutz R, Gaedicke C, Berglar K, Schloemer S, Franke D, Djajadihardja YS (2011) Petroleum systems of the Simeuleue fore-arc basin, offshore Sumatra. *Indonesia AAPG Buletin* 95(9):1589–1616
- Majumdar U, Cook AE (2018) The volume of gas hydrate-bound gas in the northern Gulf of Mexico. *Geochem Geophys Geosyst* 19(11):4313–4328
- de Man E, Ashby F, Bacheller III J, Cahyono AB, Suriamin S, Corhay J, Hillcock P, Wilmet S (2011) Deep-water site investigation - Makassar Straits (Indonesia). Proceedings Indonesian Petroleum Association 35th Annual Convention.
- Markl RG, Bryan GM, Ewing JI (1970) Structure of the Blake-Bahama Outer Ridge. *Journal Geophysical Research* 75:4539–4555
- McKirdy DW, Cook PJ (1980) Organic geochemistry of Pliocene-Pleistocene calcareous sediments, DSDP Sites 262. *Timor Trough AAPG Bull* 64(2):2118–2138
- McVeigh D, Skarke A, Dekas AE, Borrelli C, Hong WL, Marlow JJ, Pasulka A, Jungbluth SP, Barco RA, Djurhuus A (2018) Characterization of benthic biogeochemistry and ecology at three methane seep sites on the Northern U.S. Atlantic margin. *Deep Sea Res Part II* 150:41–56
- Monteleone V, Marín-Moreno H, Bayrakci G, Best A, Shaon F, Hossain MM, Karim AA, Alam MK (2022) Seismic characterization and modelling of the gas hydrate system in the northern Bay of Bengal. *Mar Pet Geol* 141:105690
- Mukti M, Singh SC, Deighton I, Hananto ND, Moeremans R, Permana H (2012) Structural evolution of backthrusting in the Mentawai Fault Zone, offshore Sumatran forearc. *Geochem Geophys Geosyst* 13:Q12006
- Neben S, Hinz K, Beiersdorf H (1998) Reflection characteristics, depth and geographical distribution of bottom simulating reflectors within the accretionary wedge of Sulawesi. *Geol Soc London Spec Public* 137:267–274
- Ning X, Shiguo W, Buqing S, Bing L, Liangqing X, Xiujuan W, Ying J (2009) Gas hydrate associated with mud diapir in southern Okinawa Trough. *Mar Pet Geol* 26:1413–1418
- Nur'Aini S, Hall R, Elders CF (2005) Basement architecture and sedimentary fills of the North Makassar Straits basin. Proceedings Indonesian Petroleum Association 30th Annual Convention.
- Nurusman S, Subono S (1995) Heat flow measurements in Indonesia. In: Gupta ML, Yamano M (Eds) Terrestrial heat flow and geothermal energy in Asia. Oxford & IBH Pub. Co., Cornell University, pp 145–162
- Peng DY, Robinson DB (1976) A new two-constant equation of state. *Industrial Ad Engineering Chemistry Fundamentals* 27:59–64
- Priyanto B, Hokstad K, Zwach C, van Schaack M, Mjos R, Hartadi ET, Tasarova ZA, Duffaut K (2015) Heat flow estimation from BSR: An example from the Aru region, offshore West Papua, Eastern Indonesia. In: Proceedings Indonesian Petroleum Association 39th Annual Convention.
- Prouty NG, Sahy D, Ruppel CD, Roark EB, Condon D, Brooke S, Ross RW, Demopoulos AWJ (2016) Insights into methane dynamics from analysis of

- authigenic carbonates and chemosynthetic mussels at newly discovered Atlantic Margin seeps. *Earth Planet Sci Lett* 449:332–344
- Ruppel CD, Kessler JD (2017) The interaction of climate change and methane hydrates. *Review of Geophysics* 55(1):1260168
- Sassen R, Curiale JA (2006) Microbial methane and ethane from gas hydrate nodules of the Makassar Strait, Indonesia. *Org Geochem* 37:977–980
- Satyana AH, Marpaung LP, Purwaningsih MEM, Utama MK (2007) Regional gas geochemistry of Indonesia: Genetic characterization and habitat of natural gases. In: Proceedings Indonesian Petroleum Association 31st Annual Convention.
- Schmidt GA, Shindell DT (2003) Atmospheric composition, radiative forcing, climate change as a consequence of a massive methane release from gas hydrates. *Paleoceanography* 18(1):1004
- Schnurle R, Hsiuan TH, Liu CS (1999) Constraints on free gas and gas hydrate bearing sediments from multi-channel seismic data, offshore southwestern Taiwan. *Petroleum Geology of Taiwan* 33:21–42
- S&P Global Commodity Insights. 2023. Another deep-water success in Indonesia: Eni's Geng North Discovery to revive ultra-deep water exploration and gas production in the Kutei Basin. IHS Markit. <https://www.spglobal.com/commodityinsights/en/ci/research-analysis/another-deepwater-success-in-indonesia.html> (Accessed 10 Jan 2024).
- Tan L, Liu F, Huang Y, Wang R, Geng J, Crosta G, Frattini P (2023) Mapping submarine landslides susceptibility in continental slopes with rich gas hydrates. *Gas Sci Eng* 116:205054
- Tharimela R, Filipov A (2018) Gas hydrate mapping using 3D CSEM. AAPG Asia Pacific Region – The 4th AAPG/EAGE/MGS Myanmar Oil and Gas Conference.
- Thompson M, Remington C, Purnomo J, MacGregor D (1991) Detection of liquid hydrocarbon seepage in Indonesian offshore frontier basins using airborne laser fluorosensor (ALF) the results of a Pertamina / BP joint study. Proceedings Indonesian Petroleum Association 20th Annual Convention.
- United Nations (2022) Enhanced Nationally Determined Contribution of Indonesia, United Nations Framework Convention on Climate Change (UNFCCC). https://unfccc.int/sites/default/files/NDC/2022-09/23.09.2022_Enhanced%20NDC%20Indonesia.pdf (Accessed 1 Dec 2023)
- Waite WF, Stern LA, Kirby SH, Winters WJ, Mason DH (2007) Simultaneous determination of thermal conductivity, thermal diffusivity and specific heat in sl methane hydrate. *Geophys J Int* 169(2):767–774
- Wood W, Gettrust J, Chapman N, Spence GD, Hyndman RD (2002) Decreased stability of methane hydrates in marine sediments owing to phase-boundary roughness. *Nature* 420:656–660
- Wyllie MRJ, Gregory AR, Gardner LW (1956) Elastic wave velocities in heterogeneous and porous media. *Geophysics* 21(1):41–70
- Wynn RB, Stow DAV (2002) Classification and characterisation of deep-water sediment waves. *Mar Geol* 192(1):7–22
- Xia Y, Yang J, Chen Y, Lu S, Wang M, Deng S, Yao Z, Lu M (2022) A review of the global polygonal faults: Are they playing a big role in fluid migration? *Front Earth Sci* 9:786915
- Xu W, Germanovich LN (2006) Excess pore pressure resulting from methane hydrate dissociation in marine sediments: A theoretical approach. *J Geophys Res* 111:B01104
- Yamamoto K (2022) Gas hydrate drilling in the Nankai Trough, Japan. In: Mienert J, Berndt C, Tréhu AM, Camerlenghi A, Liu CS (Eds) *World atlas of submarine gas hydrates in continental margins*. Springer Nature, Berlin
- Yergin D (1991) *The Prize*. Simon and Schuster. 877 p.
- You K, Kneafsey TJ, Flemings PB, Polito P, Bryant SL (2015) Salinity-buffered methane hydrate formation and dissociation in gas-rich systems. *J Geophys Res* 120:643–661
- You K, Flemings PB, Malinverno A, Collett TS, Darnell D (2019) Mechanisms of methane hydrate formation in geological systems. *Rev Geophys* 57(4):1146
- Zeng Z, Zhu H, Yang X, Cao X (2022) Three-dimensional seismic analysis of a polygonal fault system (PFS) in the Northern Carnarvon Basin, Australia: Implications for fluid flow migration and gas hydrate system. *J Petrol Sci Eng* 215:110602
- Zhang Z, Wright CS (2017) Hydrate reservoir using three-dimensional seismic and LWD data in Kutei basin, East Kalimantan, offshore Indonesia. *Mar Pet Geol* 84:257–273
- Zhang J, Hao T, Dong M, Wang B, Ai Y, Fang G (2021) Investigation of geothermal structure of the Sulawesi, using gravity and magnetic method. *Sci China Earth Sci* 64:278–293
- Zhang G, Wang X, Li L, Sun L, Guo Y, Lu Y, Li W, Wang Z, Qian J, Yang T, Wang W (2022) Gas hydrate accumulation related to pockmarks and faults in the Zhongjiannan Basin. *South China Sea Front Earth Sci* 10:902469

Publisher's Note

Springer Nature remains neutral with regard to jurisdictional claims in published maps and institutional affiliations.